Gastrodia elata Blume prevents dopaminergic neuron degeneration via glial Nrf2 signaling in Lrrk2-G2019S Parkinson's disease models

Yu-En Lin[1,2], Chin-Hsien Lin[3], En-Peng Ho[3], Yi-Ci Ke[3], Stavroula Petridi[4,5], Christopher J. H. Elliott[4], Lee-Yan Sheen[2,*], and Cheng-Ting Chien[1,6,*]

[1]Institute of Molecular Biology, Academia Sinica, Taipei, Taiwan

[2]Institute of Food Science and Technology, National Taiwan University, Taipei, Taiwan

[3]Department of Neurology, National Taiwan University Hospital, Taipei, Taiwan

[4]Department of Biology and York Biomedical Research Institute, University of York, York, UK

[5]Department of Clinical Neurosciences and MRC Mitochondrial Biology Unit, University of Cambridge, Cambridge CB2 0XY, UK

[6]Neuroscience Program of Academia Sinica, Academia Sinica, Taipei, Taiwan

*Correspondence:

Lee-Yan Sheen, E-mail: lysheen@ntu.edu.tw, Tel.: +886-2-3366-1572

Cheng-Ting Chien, E-mail: ctchien@gate.sinica.edu.tw, Tel.: +886-2-2789-9970

Abstract

Background: Parkinson's disease (PD) remains an incurable neurodegenerative disease. The most frequent missense mutations in familial PD occur in the highly conserved *LRRK2/PARK8* gene. Both fly and mouse models of PD carrying the *LRRK2* transgene with a dominant G2019S mutation exhibit locomotion defects and loss of dopaminergic neurons. *Gastrodia elata* Blume (GE) is an herbal medicine traditionally used to treat neurological diseases and has been reported to have neuroprotective effects in toxin-induced PD models. However, the underpinning molecular mechanisms of GE beneficiary to G2019S-induced PD remain unclear.

Methods: We pharmacologically treated the *Drosophila* G2019S model with water extract of GE (WGE) to evaluate the neuroprotective and locomotion-improving effects. The biochemical analyses and genetic manipulations were further applied to dissect the potential molecular pathways involved in WGE treatment. We also validated the effects and mechanisms of WGE in a G2019S transgenic mouse model.

Results: We show that these G2019S mutant flies fed with WGE showed improved locomotion and stable dopaminergic neurons. WGE suppressed the accumulation and hyperactivation of G2019S mutant protein in dopaminergic neurons, and activated the antioxidation and detoxification factor Nrf2 in glia. Activated Nrf2 antagonizes G2019S-induced Mad/Smad signaling in glia. The effects of WGE on the *Drosophila* G2019S model were recapitulated in a G2019S transgenic mouse.

Conclusion: We conclude that WGE prevents locomotion defects and the neuronal loss induced by G2019S mutation via glial Nrf2 upregulation, unveiling a potential therapeutic avenue for PD.

Keywords: Parkinson's disease, Lrrk2, *Gastrodia elata* Blume, *Drosophila*, dopaminergic neuron, Nrf2,

BMP/Mad, glia

Background

Parkinson's disease (PD) is a highly prevalent neurodegenerative disorder characterized by the loss of dopaminergic neurons in the substantia nigra projecting to the striatum of the basal ganglion, representing a circuit involved in motor planning and coordination. As a consequence, PD is associated with motor abnormalities, bradykinesia, hypokinesia, rigidity and resting tremor. Currently, the most frequently applied pharmacological treatment, levodopa (L-DOPA), exerts limited motor improvement and elicits negative side-effects [1]. Hence, identifying and developing alternative or complementary treatments may assist in mitigating PD progression.

PD is a multi-causal disease with a complicated etiology, including familial inheritance. More than 20 *PARK* genes have been genetically linked to PD, a number that is increasing [2]. Missense mutations in *PARK8*, or *Leucine-rich repeat kinase 2* (*LRRK2*) induce characteristic PD symptoms and pathologies such as loss of dopaminergic neurons and the appearance of Lewy bodies [3]. Notably, the most commonly observed mutation, dominant G2019S, among familial PD cases is located in the kinase domain of Lrrk2, which augments its kinase activity via auto- and hyper-activation [4]. The hyperactive G2019S mutant protein alters several cellular processes including vesicle trafficking, microtubule dynamics, autophagy, and mitochondrial function, contributing to neuronal degeneration [3].

Glia provide structural and metabolic supports to neurons and regulate synaptic transmissions, so they are important for the function and survival of dopaminergic neurons [5, 6]. Dysfunctional astrocytes and microglia, two major glial types, contribute to onset and progression of both sporadic and familial PD [7]. Astrocytes and microglia of postmortem PD brains exhibit pathologic lesions and hyper-immunoactivity [8].

Clinical trials involving glia-derived neurotropic factor (GDNF) delivery or modulation of glial oxidative stress highlight the significance of glia to PD [9, 10]. Moreover, Lrrk2 regulates the inflammatory response in microglia and the autophagy-lysosome pathway in astrocytes, with the G2019S mutation altering the size and pH of lysosomes [11, 12]. These studies indicate that mutated Lrrk2 alters the homeostasis and interaction between neurons and glia, contributing to PD pathogenesis.

Given that up to 70% of human *PARK* genes are conserved in the *Drosophila* genome, *Drosophila* is frequently used as a PD model for studying gene function, such as the *PARK1/SNCA* [13] and *PARK8/LRRK2* [14]. Genetic and molecular linkage between *PINK1/PARK6* and *Parkin/PARK2* was first established in *Drosophila* [15]. When overexpressed in *Drosophila* dopaminergic neurons, *Lrrk2* transgenes carrying G2019S or other dominant mutations induce dopaminergic neuron loss and locomotion impairment, two age-dependent symptoms of PD [14, 16]. The G2019S model has further been used to screen a collection of FDA-approved drugs to suppress these PD phenotypes. Strikingly, lovastatin was found to prevent dendrite degeneration, dopaminergic neuron loss, and impaired locomotion and, critically, a lovastatin-involved pathway proved neuroprotective [17]. Thus, *Drosophila* represents an amenable model of PD for genetic, molecular and pharmacological study of potential therapeutic interventions.

Traditional Chinese Medicine (TCM) is often used as a complementary treatment for human diseases, including PD [18, 19]. Although the results were inconclusive, some TCM could display adjuvant effects when used in combination with L-DOPA, reducing the L-DOPA dosage required in long-term treatments and relieving non-motor symptoms [18]. As a prominent component in TCM, *Gastrodia elata* Blume (GE; Orchidaceae) has been used to treat neurological disorders for centuries [20]. GE has been shown to exert

neuroprotective, anti-inflammatory and antioxidative effects in neurodegenerative disease models [21]. GE genome sequencing analysis has indicated that symbiosis between GE and the fungus *Armillaria mellea* (Physalacriaceae) benefits nutrient uptake and synthesis of bioactive compounds [22]. The major bioactive compounds generated include gastrodin and 4-hydroxybenzyl alcohol (4-HBA), both of which display pharmacological effects on neurobiological and psychological disorders [23, 24]. Moreover, GE ameliorates the drug-induced dyskinesia caused by prolonged L-DOPA treatment in rodents [25], highlighting a potential benefit of incorporating GE in PD treatments. However, the molecular and cellular mechanisms underlying how GE can moderate PD or other neurological disorders remain unclear.

We have investigated the impact of GE treatment on PD in restoring locomotion and protecting dopaminergic neurons in the *Drosophila* G2019S model. We identified two distinct pathways induced by GE in the model, i.e., suppression of Lrrk2 protein accumulation and hyperphosphorylation in neurons, and activation of the nuclear factor-erythroid factor 2-related factor 2 (Nrf2) pathway in glia. Expression of G2019S mutant protein in neurons was previously shown to induce the secretion of Glass bottom boat (Gbb)/ bone morphogenetic proteins (BMP) signal that, in turn, upregulates Mothers against decapentaplegic (Mad)/Smad signaling in glia, which prompts feedback signals to promote neuronal degeneration [26]. We show that GE-induced Nrf2 activation antagonizes the Gbb-activated Mad signaling in glia, contributing to neuronal protection. GE also antagonized Smad2/3 signaling in a G2019S mouse model, which restored locomotion and protected dopaminergic neurons. Conservation of the pathways impacted by GE treatment in both the *Drosophila* and mouse G2019S models implies that the beneficial

effects of GE could be conserved in human and represent a reliable and effective complementary therapy for PD.

Methods

Drosophila stocks and maintenance

All fly stocks were maintained on standard cornmeal-based food medium at 25°C. *Drosophila* stocks sourced from the Bloomington *Drosophila* Stock Center (Indiana University, Bloomington, USA) were: *UAS-mCD8-GFP* (#5137), *elav-GAL4* (#8760), *repo-GAL4* (#7215), *Ddc-LexA* (#54218), *UAS-cncTRiP* (#25984), *Tub-GAL80*^{ts} (#7108), *alrm-GAL4* (#67032), *R56F03-GAL4* (#39157), *UAS-tkv*^{Q253D} (#36536), and *Mad*^{K00237} (#10474). *NP2222-GAL4* (#112830) was from the *Drosophila* Genomics Resource Center and *NP6293-GAL4* (#105188) was from the Kyoto Stock Center. Other stocks include *UAS-Flag-LRRK2-WT* [16], *UAS-Flag-LRRK2-G2019S* [16], *Ddc-GAL4* [27], *ARE-GFP* [28], *UAS-cncC-FL2* [28], *moody-GAL4* [29], and *UAS-Mad* [30]. The two *LexAop* fly lines—*LexAop-LRRK2-WT* and *LexAop-LRRK2-G2019S*—were generated in this study. In brief, the cDNAs for *LRRK2-WT* and *LRRK2-G2019S* were isolated from plasmids (Invitrogen, California, USA) for subcloning into *LexAop* plasmids (Addgene, Massachusetts, USA), which were for microinjection (Fly facility, University of Cambridge, UK). The transgenes were site landed at an attP site on the 2nd chromosome (25C6). For temperature-shift assay of *GAL80*^{ts} flies, parental flies were maintained at 19°C and allowed to mate, before collecting the F1 adults and shifting them to 29°C to inactivate GAL80.

Preparation of WGE and related chemical compounds

Authentication of GE and preparation of WGE were as described previously [23, 31]. WGE (KO DA Pharmaceutical Co. Ltd., Taoyuan, Taiwan), gastrodin (Wuhan YC Fine Chemical Co., Wuhan, China), and

4-HBA (Sigma-Aldrich, Darmstadt, Germany) were added to freshly-prepared cornmeal-based fly food at indicated final concentrations (w/w). For experiments, one- to three-day-old post-eclosion flies were collected and transferred to fresh food medium twice per week.

Fly locomotion assay

A negative geotaxis climbing assay was performed to assess locomotor activity, and it was conducted according to a previous study with minor modification [32]. Cohorts of 35 flies from each genotype were assayed weekly for six consecutive weeks. Success rates were calculated as the percentage of flies that could climb above the 8-cm mark of a 20-cm cylinder within 10 s.

The free-walking assay protocol was conducted based on a previous report with minor modification [33]. Cohorts of eight flies were habituated on a 10-cm agar-filled dish for 30 min. The dishes were gently tapped to encourage the flies to walk, which was video-taped for 5 min. Movement tracks were processed in ImageJ and quantified using the Caltech multiple fly tracker (Ctrax).

Immunostaining and immunoblotting of adult fly brains

The protocol for immunostaining whole-mount adult brains was essentially as described previously [16, 26]. Adult fly brains for each genotype were dissected at the indicated time-points for immunostaining with the following primary antibodies: mouse anti-tyrosine hydroxylase (TH) (Immunostar, 22941, 1:1000); mouse anti-repo (Hybridoma Bank DSHB, 8D12, 1:500); chicken anti-GFP (Abcam, ab13970, 1:10000); and rabbit anti-phospho-Smad3 (Ser423/425) (Abcam, ab52903, 1:250) [34]. Fluorophore-conjugated

secondary antibodies were: FITC-conjugated goat anti-mouse IgG (Jackson Lab, AB_2338589, 1:500); Alexa Fluor 488-conjugated goat anti-mouse IgG (Invitrogen, A28175, 1:500); Cy3-conjugated goat anti-mouse IgG (Jackson Lab, AB_2338680, 1:500); Alexa Fluor 488-conjugated goat anti-rabbit IgG (Invitrogen, A27034, 1:500); and Cy5-conjugated goat anti-rat IgG (Invitrogen, A10525, 1:500). Phalloidin-TRITC (Sigma, P1951, 1:5000) that binds F-actin was also used for counterstaining. Immunofluorescence signals were acquired under confocal microscopy (ZEISS LSM 710, Germany).

Adult brain extracts were prepared according to a previously described protocol [16]. In brief, ~80 fly heads for each genotype were isolated for extract preparation. Equivalent amounts of samples (30 μg/20 μL/well) were resolved by SDS-PAGE for immunoblotting. The following primary antibodies were used: rabbit anti-human LRRK2 (Abcam, ab133474, 1:1000); rabbit anti-phospho-LRRK2 (Ser^{1292}) (Abcam, ab203181, 1:500); rabbit anti-Akt (Cell Signaling, #4691, 1:1000); rabbit anti-*Drosophila* phospho-Akt Ser^{505} (Cell Signaling, #4054, 1:500); rabbit anti-Nrf2 (Thermo, 710574, 1:1000); rabbit anti-phospho-Nrf2 (Ser^{40}) (Thermo Fisher Scientific, PA5-67520, 1:1000); mouse anti-HO-1-1 (Thermo Fisher Scientific, MA1-112, 1:1000); rabbit anti-GAPDH (GeneTex, GTX100118, 1:5000); and rabbit anti-alpha tubulin (Cell Signaling, #2144, 1:10000), followed by blotting with secondary antibodies peroxidase-conjugated goat anti-rabbit IgG (Jackson Lab, AB_2307391, 1:7500) and peroxidase-conjugated goat anti-mouse IgG (Jackson Lab, AB_10015289, 1:7500).

***ARE-GFP* reporter assay**

The antioxidant response element (*ARE)-GFP* reporter assay was a modification of the protocol from a

previous study [28]. One-day old virgin female flies (homozygous for *ARE-GFP*) were mated for one day, and then fed with regular food or food containing 0.1% WGE for two more days before imaging for GFP signals. To immunostain the *ARE-GFP* reporter signal in brain, feeding of 0.1% WGE was extended to 5 days. To quantify *ARE-GFP* in adult fly brain, the 0.5-μm confocal images were processed in ImageJ. Mean *ARE-GFP* fluorescence intensities of *mCherry*-labeled glial cells in the PPL1 neuronal cluster were quantified by manually outlining the labeled area to first measure mean GFP signal and then normalizing it to mCherry signal (GFP/mCherry).

Animal care and treatments

Transgenic *LRRK2-G2019S* mice were purchased from Jackson Laboratory (JAX stock #009609, Bar Harbor, ME, USA) and they were maintained at the animal center of the National Taiwan University Hospital (NTUH). Non-transgenic (nTg) and heterozygous transgenic *LRRK2-G2019S* mice were obtained by crossing heterozygous *LRRK2-G2019S* mice with wild-type FVB/NJ mice. Mice at 8.5 months-old were assigned to one of three groups (5 to 6 mice per group): nTg, *LRRK2-G2019S*, and *LRRK2-G2019S* fed with WGE (0.5 g/kg body weight per day) [31] for three months.

Behavioral assays

We employed two behavioral tests to assay mouse motor function, i.e., an open field assay to assess spontaneous locomotor activity and CatWalk XT gait analysis to assay coordination. Behavioral experiments were conducted blind to genotype, as described previously [35, 36].

Immunohistochemical staining

After three months of WGE treatment, mice were sacrificed at the age of 11.5 months. The substantia nigra and striatum were dissected out. The substantia nigra was subjected to immunostaining, as described previously [35]. Anti-tyrosine hydroxylase (TH) (Millipore, AB152, 1:200) and anti-ionized calcium-binding adapter molecule 1 (Iba-1) (GeneTex, GTX100042, 1:200) were used as primary antibodies for 24 h at 4°C. Secondary antibodies were DyLight 488 goat anti-rabbit 1:300 and DyLight 546 goat anti-rabbit at 1:200 (25°C for 1 h). Mounting medium with DAPI (GeneTex, GTX30920) was used as a counterstain.

Immunoblotting

Frozen nigrostriatal brain tissues were homogenized and mixed with lysis buffer to determine protein content and for immunoblotting, as described previously [35]. The membrane was incubated overnight at 4°C with the following primary antibodies: anti-LRRK2 (Abcam, ab133474, 1:5000); anti-phospho-LRRK2 (Ser^{935}, Abcam, ab133450, 1:1000); anti-phospho-LRRK2 (Ser^{1292}, Abcam, ab203181, 1:1000); anti-Smad2 (Cell Signaling, 5339T, 1:1000); anti-phospho-Smad2 (Ser465/467, Cell Signaling, 3108T, 1:1000); anti-Smad3 (Cell Signaling, 9523T, 1:1000); anti-phospho-Smad3 (Ser423/425, Abcam, ab52903, 1:1000); and anti-beta actin (Sigma-Aldrich, A5441, 1:5000). After washing, peroxidase-conjugated goat anti-rabbit IgG (GeneTex, GTX213110-01, 1:5000) or peroxidase-conjugated goat anti-mouse IgG (GeneTex, GTX213111-01, 1:5000) were used as secondary antibodies.

Data analysis

All statistical analyses were carried out in GraphPad PRISM 6 (La Jolla, CA, USA). Data are presented as mean ± standard error (SEM). Statistical analysis was performed using either student *t*-test or one-way analysis of variance (ANOVA) followed by Tukey's multiple comparison test. *P* values less than 0.05 ($p < 0.05$) were considered indicative of significance.

Results

WGE treatment improves locomotion of *Ddc>G2019S* flies.

We employed the *GAL4-UAS* system to express the G2019S mutant of Lrrk2 by the *Ddc-GAL4* driver (*Ddc>G2019S*) in dopaminergic neurons and then assessed the anti-geotactic climbing activity of adult flies. We observed that locomotion of *Ddc>G2019S* flies was affected significantly relative to control flies expressing wild-type Lrrk2 (*Ddc>Lrrk2*) (Fig. 1a, Supplementary Fig. 1a). At weeks 1 and 2, more than 80% of *Ddc>G2019S* flies could successfully climb above an 8-cm threshold, a proportion comparable to that of *Ddc>Lrrk2* flies. However, the success rate declined to ~40% at week 3, ~20% at week 4, and to less than 10% at weeks 5 and 6. These proportions are significantly lower than the ~80% at week 3, ~60% at week 4, and ~40% at weeks 5 and 6 displayed by *Ddc>Lrrk2* flies. Although both *Ddc>G2019S* and *Ddc>Lrrk2* flies failed to reach the 8-cm mark at weeks 7 and 8, *Ddc>Lrrk2* flies could still climb the wall, whereas almost all *Ddc>G2019S* flies could not (Supplementary Fig. 1a). We also tested the climbing activity of another control expressing GFP in dopaminergic neurons (*Ddc>mCD8-GFP*). Both *Ddc>Lrrk2* and *Ddc>mCD8-GFP* flies showed comparable climbing activities in the first six weeks, and a significant number of *Ddc>mCD8-GFP* flies were still able to climb above the 8-cm mark at week 7. Therefore, we used the *Ddc>Lrrk2* line as a control for *Ddc>G2019S* flies in subsequent experiments to dissect the specific mode of pathogenicity of the G2019S mutation.

Next, we examined the effect of feeding flies with water extracts of GE (WGE) as a food supplement at different concentrations (0.1, 0.5 or 1.0%, w/w). WGE treatment of *Ddc>G2019S* flies at all three doses elicited a significant improvement in their climbing ability (Fig. 1a). Strikingly, the lowest concentration

(0.1%) of WGE proved the most effective, with *Ddc>G2019S* flies still performing well at climbing (i.e., comparably to *Ddc>Lrrk2* control flies) in weeks 5 and 6. The higher doses of WGE (0.5 % and 1.0%) still exerted beneficial effects at weeks 3 and 4, albeit not as significantly as the 0.1% dose, but had no beneficial effect in weeks 5 and 6. As 0.1% is the lowest among the three doses tested, we lowered the dose of WGE to 0.02% and found that 0.02% WGE was less effective than 0.1% starting at week 3 till week 6, suggesting that 0.1% is the optimal does in restoring the climbing activity of *Ddc>G2019S* flies (Supplementary Fig. 1b).

Gastrodin and 4-HBA are two major phenolic compounds in GE displaying neuropharmacological effects [37]. Feeding *Ddc>G2019S* flies with food containing gastrodin (0.1 mM) equivalent to the amount in 0.1% WGE also restored locomotion of *Ddc>G2019S* flies in weeks 2-4, though its impact diminished to non-significant levels at weeks 5 and 6. However, increasing the gastrodin dose ten-fold (1.0 mM) resulted in improved climbing activity at weeks 5 and 6 (Fig. 1b). Similarly, the equivalent 0.1 mM of 4-HBA, the aglyconic form of gastrodin and the bioactive form in the brain [38], was sufficient to restore the climbing ability of *Ddc>G2019S* flies, and a ten-fold dose at 1.0 mM had an even better effect (Fig. 1c). These results indicate that both gastrodin and 4-HBA are primary bioactive compounds in GE that prevent locomotion decline in *Ddc>G2019S* flies, and higher doses are more beneficial to reach the effect as WGE did.

Success in the anti-gravity wall-climbing assay also requires an immediate response to startle knockdown. Accordingly, we performed a second assay, free-walking in an open arena, to assess improved locomotion. Consistently, free-walking by *Ddc>G2019S* flies was greatly impaired, with total walking

distance reduced to less than 20% that displayed by control *Ddc>Lrrk2* flies (Fig. 1d). Moreover, *Ddc>G2019S* flies displayed centrophobism, i.e., they avoided walking into the central open space. Strikingly, 0.1% WGE feeding greatly extended walking distance and suppressed the centrophobism of *Ddc>G2019S* flies. Together, these two assays strongly indicate that the defective locomotion exhibited by *Ddc>G2019S* flies is greatly improved by feeding them with 0.1% WGE. We therefore fed the flies with 0.1% WGE in the following experiments.

WGE treatment suppresses dopaminergic neuron loss in *Ddc>G2019S* brain.

Expression of G2019S mutant protein has been shown to induce a gradual loss of dopaminergic neurons in the adult fly brain, contributing to impaired locomotion [14, 16]. Several clusters of dopaminergic neurons have been identified in the adult brain of *Drosophila*. Here, we focused on the PPL1, PPL2, PPM1/2 and PPM3 clusters that have well-defined roles in modulating locomotion [39] to assess the effect of WGE treatment. We detected reduced numbers of dopaminergic neurons in the PPL1, PPL2, PPM1/2, and PPM3 clusters of *Ddc>G2019S* flies relative to *Ddc>Lrrk2* controls, which increased in severity from week 2 to 6 (Fig. 2, Supplementary Fig. 2). Consistently, feeding *Ddc>G2019S* flies with 0.1% WGE restored numbers of dopaminergic neurons in these clusters to the levels observed in controls (Fig. 2, Supplementary Fig. 2). Thus, concomitant rescue of locomotion and dopaminergic neuron populations in *Ddc>G2019S* flies indicates that WGE treatment likely promotes dopaminergic neuron survival to restore locomotion.

WGE treatment suppresses G2019S-induced Lrrk2 hyperactivation.

The enhanced survival of dopaminergic neurons due to WGE treatment implies that WGE induces neuroprotective mechanisms in *Ddc>G2019S* flies. The G2019S mutation causes Lrrk2 hyperphosphorylation, protein accumulation, and aberrant cellular signaling [40]. Therefore, we explored if WGE-induced neuroprotection is responsible for abrogating these processes in mutant flies. We detected comparable levels of Lrrk2 proteins in newly eclosed adult brains pan-neuronally expressing wild-type Lrrk2 (*elav>Lrrk2*) or G2019S mutant protein (*elav>G2019S*) (Fig. 3a). However, phosphorylation levels at the Ser^{1292} autophosphorylation site was higher in the *elav>G2019S* flies compared to *elav>Lrrk2* (Fig. 3a, b). This outcome was also observed at week 4 (Fig. 3f, g), consistent with the idea that Lrrk2 is hyperactivated upon G2019S mutation. Hyperphosphorylation in *elav>G2019S* flies led to Lrrk2 protein accumulation, as determined by total Lrrk2 levels at weeks 2 and 4 (Fig. 3d, e). However, both hyperphosphorylation and protein accumulation were suppressed upon feeding *elav>G2019S* flies with 0.1% WGE (Fig. 3d-g). In the *elav>Lrrk2* control, WGE feeding had no effect on levels of wild-type Lrrk2 or Ser^{1292} phosphorylation (Supplementary Fig. 3a-c). We further examined the G2019S mutant-activated downstream effector Rab10, the phosphorylation status of which can serve as an indicator of Lrrk2 kinase activity [41]. We observed that levels of phosphorylated Rab10 were increased in *elav>G2019S* flies, but this phenotype was suppressed by WGE feeding (Fig. 3f, h). Hence, feeding flies with WGE suppresses G2019S-induced Lrrk2 protein phosphorylation, accumulation, and signaling.

WGE treatment restores Akt/GSK3β/Nrf2 pathway activity.

The protein kinase B (Akt)/Glycogen synthase kinase 3β (GSK3β)/Nuclear factor-erythroid factor 2-related factor 2 (Nrf2) signaling axis has been shown to promote survival of dopaminergic neurons and ameliorate motor dysfunction in PD models [42]. We assayed the phosphorylation status of Akt at Ser^{505} in newly eclosed adult fly head extracts and found reduced levels of pAkt in *elav>G2019S* flies relative to *elav>Lrrk2* controls (Fig. 3a, c). This pAkt reduction persisted at weeks 2 and 4, but was abrogated by feeding *elav>G2019S* flies with 0.1% WGE (Fig. 4a, b). We also examined phosphorylation levels of Nrf2 at Ser^{40} and GSK3β at Ser^{9}, both of which were reduced upon expression of G2019S mutant protein and were equally offset by WGE feeding (Fig. 4c, d). Induction of Akt/GSK3β/Nrf2 signaling activates expression of heme oxygenase 1 (HO-1), and we observed diminished levels of this latter protein in *elav>G2019S* flies, which could be rescued by WGE feeding (Fig. 4c, d). Therefore, WGE feeding restores the Akt/GSK3β/Nrf2 signaling activity compromised by the G2019S mutation.

Glial Nrf2 mediates the beneficial effect of WGE on restored locomotion and neuronal protection in *G2019S* mutant flies.

Restoration of Akt/GSK3β/Nrf2 signaling activity by WGE treatment prompted us to test by genetic assays if that signaling pathway mediates the WGE mode of action. We focused on the downstream effector Nrf2 encoded by *cap-n-collar* (*cnc*) in *Drosophila*. Intriguingly, neither overexpression (*UAS-cncC-FL2*) nor RNAi knockdown (*UAS-cncTRiP*) of Nrf2 in dopaminergic neurons had an impact on the climbing ability of *Ddc>G2019S* flies (Fig. 5a). Also, WGE feeding still rescued locomotion of *Ddc>G2019S* flies with Nrf2 knockdown (*Ddc>G2019S; cncTRiP*) to levels comparable to WGE-fed control flies

(*Ddc>G2019S; mCD8-GFP*) without Nrf2 knockdown (Fig. 5a). Thus, the Nrf2 pathway activation by WGE that appears to be effective in protecting neurons and restoring locomotion is likely exerted in cells other than neurons.

Nrf2 activation may be examined by assessing GFP signal from the *ARE-GFP* reporter that harbors Nrf2 binding sites and responds to Nrf2 activation [43]. *ARE-GFP* adult fly brains displayed low basal GFP signals (Fig. 5c), but feeding with 0.1% WGE elicited many GFP-positive signals in Repo-positive glia (arrowheads in Fig. 5d), evidencing that glia may be the primary cell type in which Nrf2 is activated.

Next, we investigated if WGE-induced Nrf2 activity in glia is effective in promoting locomotion in G2019S flies. To this end, we employed the *LexA-LexAop* system to overexpress wild-type Lrrk2 or G2019S mutant protein in dopaminergic neurons (*Ddc-LexA>Lrrk2* and *Ddc-LexA>G2019S*, respectively), and used the *GAL4* driver to manipulate Nrf2/CncC activity in glia (*repo>cncC-FL2* for overexpression and *repo>cnc-RNAi* for knockdown). As a first step, we validated the age-dependent locomotion decline of *Ddc-LexA>G2019S* flies that was severer than *Ddc-LexA>Lrrk2* and could be rescued by 0.1% WGE feeding (Supplementary Fig. 4). We then assayed the climbing ability of *Ddc-LexA>G2019S* flies exhibiting *repo-GAL4*-driven Nrf2 overexpression in glia (*Ddc-LexA>G2019S; repo>cncC-FL2*). Significantly, the *Ddc-LexA>G2019S; repo>cncC-FL2* flies performed better in the climbing assay than *Ddc-LexA>G2019S; repo-GAL4* without Nrf2 overexpression (Fig. 5b). We also performed Nrf2 knockdown in glia (*Ddc-LexA>G2019S; repo>cnc-RNAi*), which had little impact on the already declined climbing activity in *Ddc-LexA>G2019S; repo-GAL4* (Fig. 5b). Importantly, WGE feeding could not rescue locomotion deficits of glial Nrf2-knockdown flies (*Ddc-LexA>G2019S; repo>cnc-RNAi*) (Fig. 5b, compare

to *Ddc-LexA>G2019S; repo-GAL4* with WGE feeding). Thus, glial overexpression of Nrf2 partially restores locomotion of *Ddc-LexA>G2019S* flies, and glial depletion of Nrf2 abolishes the ability of WGE to rescue impaired locomotion.

We stained dopaminergic neurons of 6-week-old adult fly brains and confirmed that numbers of TH-positive dopaminergic neurons in the PPL1 cluster were reduced in the *Ddc-LexA>G2019S; repo-GAL4* flies compared to *Ddc-LexA>Lrrk2*; *repo-GAL4* controls (Fig. 5e, f). Importantly, numbers of dopaminergic neurons in the PPL1 cluster were restored upon glial overexpression of Nrf2 in the *Ddc-LexA>G2019*S; *repo>cncC-FL2* flies. In contrast, glial Nrf2 knockdown had little impact on the already reduced dopaminergic neurons. Taken together, these results support that glial Nrf2 is compromised in *Ddc-LexA>G2019S* flies, and glial expression of Nrf2 protects the dopaminergic neurons.

Although WGE feeding suppressed hyperactivity of G2019S mutant protein (Fig. 3d-g), it was not clear if WGE-mediated Nrf2 activation in glia could directly suppress mutant protein hyperactivity in dopaminergic neurons. To test this possibility, we compared the levels of total Lrrk2 protein and phosphorylated Lrrk2 protein in *Ddc-LexA>G2019S* with and without glial Nrf2 overexpression (*Ddc-LexA>G2019S; repo-GAL4* and *Ddc-LexA>G2019S; repo>cncC*). We observed comparable levels of Lrrk2 and pLrrk2 in the control and Nrf2 overexpression lines (Supplementary Fig. 5a-c). Thus, the neuroprotective effects of Nrf2 activity are unlikely to operate through modulation of Lrrk2 levels or activity.

Nrf2 in astrocyte-like and ensheathing glia are the major targets of WGE that alleviate *Lrrk2-G2019S*

locomotion deficits.

Five types of glia with different morphologies and functions have been identified in the fly brain [44]. We decided to identify specific subtypes of glia that may mediate the WGE-induced Nrf2 activity endowing neuronal protection, given that dysfunctional astrocytes and microglia have been linked to onset and progression of both sporadic and familial PD [7]. In *Ddc-LexA>G2019S* flies, *GAL4*-driven *cnc* knockdown in astrocyte-like (*Ddc-LexA>G2019S; alrm>cnc-RNAi*) or ensheathing glia (*Ddc-LexA>G2019S; R56F03>cnc-RNAi*) abolished the improved locomotion elicited by WGE treatment, recapitulating the effect of pan-glial Nrf2 knockdown (*Ddc-LexA>G2019S; repo>cnc-RNAi*) (Fig. 6a). This outcome was not observed when we used GAL4 drivers to knock down *cnc* in cortex (*np2222*), perineurial (*np6293*), or subperineurial (*moody*) glia. We confirmed the involvement of astrocyte-like and ensheathing glia by means of Nrf2 overexpression in astrocyte-like (*Ddc-LexA>G2019S; alrm>cncC-FL2*) or ensheathing (*Ddc-LexA>G2019S; R56F03>cncC-FL2*) glia, with both treatments improving the climbing activity of *Ddc-LexA>G2019S* flies not subjected to WGE feeding (Fig. 6b). These analyses indicate that WGE feeding induces Nrf2 activity in astrocyte-like and ensheathing glia, which mitigates the reduced locomotion displayed by G2019S mutant-expressing flies.

Next, we assayed Nrf2-regulated *ARE-GFP* expression in astrocyte-like and ensheathing glia of flies expressing G2019S mutant protein and subjected to WGE treatment. We focused on the astrocyte-like and ensheathing cells located adjacent to dopaminergic neurons. In control flies expressing wild-type Lrrk2, we detected basal levels of GFP signal in mCherry-positive astrocyte-like (*alrm-GAL4*) or ensheathing glia (*R56F03*) (Fig. 6c-f). We detected lower levels of GFP signal in these cells when G2019S mutant protein

was expressed in dopaminergic neurons. However, upon feeding with 0.1% WGE, we observed higher levels of GFP signal in both types of glia. Thus, overexpression of G2019S mutant protein in dopaminergic neurons elicited reduced Nrf2 signaling activity, but WGE feeding restored or further enhanced Nrf2 activities in these two glial subtypes.

Nrf2 activation antagonizes BMP signaling in glia.

G2019S mutant protein in dopaminergic neurons has been shown previously to enhance the expression of the proprotein convertase Furin 1 (Fur1) that processes the bone morphogenetic protein (BMP) signaling molecule Glass bottom boat (Gbb) for maturation and release, leading to activation of the BMP signaling pathway in glia [26]. We confirmed that finding by removing one copy of *Mad* that encodes the pathway's downstream effector to restore locomotion in *Ddc>G2019S* flies (Supplementary Fig. 6). To address if WGE-induced Nrf2 activation could antagonize BMP signaling activity in glia, first we assessed expression of the phosphorylated Mad (pMad) activated by BMP signaling. In glia of *Ddc>G2019S* adult fly brains, pMad levels were higher than in *Ddc>Lrrk2* brains and they could be suppressed by WGE treatment (Fig. 7a, b). Similar to the previous report [26], glial overexpression of Mad (*UAS-Mad*) or constitutively active type I receptor Tkv (*UAS-tkv*^{Q253D}) was sufficient to impair locomotion, even without expressing G2019S mutant protein in neurons. However, impaired locomotion was rescued in both cases by 0.1% WGE feeding (Fig. 7c, d). In addition, numbers of dopaminergic neurons in the PPL1 cluster were reduced upon glial overexpression of *Mad* or *tkv*^{Q253D} and they were restored by 0.1% WGE treatment (Fig. 7e-h). Together, these analyses indicate that activation of BMP signaling in glia recapitulates the phenotypes observed in

flies overexpressing G2019S mutant protein in dopaminergic neurons and, furthermore, that these effects can be suppressed by WGE treatment.

Next, we explored if WGE-induced Nrf2 activation antagonizes BMP signaling in glia. Glial Nrf2 overexpression in *Ddc-LexA>G2019S* flies (*Ddc-LexA>G2019S; repo>cncC-FL2*) partially rescued the locomotory impairment caused by G2019S mutation (Fig. 5b), and removing one copy of *Mad* (*Ddc-LexA>G2019S, Mad*$^{+/-}$*; repo>cncC-FL2*) further enhanced this effect (Fig. 8a). Indeed, this outcome was equivalent to removing one copy of *Mad* but without Nrf2 overexpression (*Ddc-LexA>G2019S, Mad*$^{+/-}$*; repo-GAL4*), suggesting that Nrf2 functions mainly to antagonize Mad activity (Fig. 8a). Consistently, Nrf2 overexpression in glia or WGE treatment suppressed the up-regulation of pMad levels in glia caused by G2019S mutant protein overexpression in dopaminergic neurons (*Ddc-LexA>G2019S; repo-GAL4*) (Fig. 8b, c). Depletion of Nrf2 from glia (*Ddc-LexA>G2019S; repo>cnc-RNAi*), even in the presence of WGE treatment, maintained high pMad levels in glia (Fig. 8b, c). Thus, modulation of Nrf2 activity, either by genetic manipulation or by WGE treatment, has an antagonistic effect on pMad levels in glia.

We also addressed if *Mad* modulates expression of the Nrf2 target *ARE-GFP*. We observed diminished GFP signal in PPL1-surrounding glia of *Ddc-LexA>G2019S* adult fly brains relative to the *Ddc-LexA>Lrrk2* control. Heterozygosity of *Mad* in *Ddc-LexA>G2019S* flies (*Ddc-LexA>G2019S, Mad*$^{+/-}$) restored the level of GFP signal, implying that Mad modulates targeted gene expression induced by Nrf2 activity (Fig. 8d, e).

The effects of WGE treatment in a *G2019S* mouse model.

To study the effect of WGE on G2019S mutation-induced neurodegeneration in a mammalian system, we fed *G2019S* mice with WGE starting at the age of 8.5 months, i.e., prior to onset of impairments in locomotion and dopaminergic neurons [45]. We quantified three locomotor activities from video-tracking paths of an open-field test, i.e., accumulative moving distance, average velocity, and percentage of time moving (Fig. 9a, b). At the age of 8.5 months, three groups—non-transgenic (nTg), transgenic *G2019S*, and WGE-fed transgenic *G2019S* mice—presented comparable locomotor activities. At 9.5 months of age, the *G2019S* mice displayed clearly impaired locomotion, which was statistically significant at the age of 11.5 months relative to nTg littermates (Fig. 9b), consistent with a previous report [46]. Importantly, the *G2019S* mice fed with WGE showed improved locomotion throughout the 3-month treatment period, an outcome that was statistically significant at 11.5 months (Fig. 9a, b). WGE treatment also suppressed the centrophobism displayed by *G2019S* mice (Fig. 9a). We also analyzed the gait of these three groups of mice (Fig. 9c). Similar to our findings from the open field test, stride length of *G2019S* mice was significantly reduced at 11.5 months, but it was restored to the level of nTg mice by WGE feeding (Fig. 9c, d). Collectively, these analyses show that WGE feeding is an effective means of restoring G2019S mutation-induced locomotory declines in this mouse model of PD.

Since the nigral-striatal system contributes to locomotor function, we counted the number of TH-positive dopaminergic neurons in the substantia nigra. In comparison to nTg littermates, the number of dopaminergic neurons in 11.5-month-old *G2019S* mice was significantly reduced, but WGE treatment for three months abrogated this loss of dopaminergic neurons (Fig. 10a, b). In the *G2019S Drosophila* model, glia mediate the protective effects of WGE on dopaminergic neurons. We found that activated microglia

marked by ionized calcium-binding adapter molecule 1 (Iba-1) were increased in the substantia nigra of *G2019S* mice, but this increase was suppressed by WGE treatment (Fig. 10c, d). We further analyzed levels of activated Lrrk2 (pLrrk2) in lysates isolated from the nigra-striatum. Levels of pLrrk2 normalized to Lrrk2 signal were higher in *G2019S* mice than in nTg littermates, but WGE treatment partially abrogated that outcome (Fig. 10e, f). Since G2019S mutation enhanced Mad signaling activation in the fly brain (Fig. 8b, c), we also tested this scenario in the mouse model. Immunoblots revealed that the ratio of phosphorylated Smad2 to total Smad2 (pSmad2/Smad2) was significantly elevated in *G2019S* mice, but this increase was suppressed by WGE treatment (Fig. 10e, g). Moreover, although the level of pSmad3/Smad3 was not significantly enhanced by G2019S mutant protein expression, it was suppressed by WGE treatment (Fig. 10e, g). Thus, WGE feeding suppresses G2019S mutation-induced microglia activation and Smad signaling in the substantia nigra of the *G2019S* mouse model of PD.

Discussion

Motor dysfunction in *Drosophila* neurodegeneration models has been frequently evaluated by means of negative-geotaxis assay that measures the insect innate response. The assay begins with a sudden external stimulation, which initially inhibits spontaneous locomotion but is followed by climbing behavior. The entire response requires motor circuit coordination and muscle tone regulation, two processes that progressively decline with age and that are impacted by neuropathological insults [47]. In contrast, the open-arena walking assay allows free exploration without disturbance, representing an assay for locomotor activities that can reveal deficits like bradykinesia [33]. Our G2019S flies exhibited reduced locomotor activity in both assays. Moreover, the mutant flies also exhibited centrophobism-like behavior in the open-arena (Fig. 1d). Centrophobism is indicative of emotional abnormalities, such as anxiety and depression, both of which are often associated with PD [48], and was also displayed by the *G2019S* mice (Fig. 9a). WGE treatment suppresses centrophobism in both fly and mouse PD models has important implications for tackling major symptoms of PD and even non-PD-related depression, as reported for rodent models [23, 31]. Thus, WGE treatment exerts beneficial effects in both of our PD models.

We found that the 0.1% dosage of WGE is optimal in suppressing age-dependent locomotion decline in G2019S flies, with higher and lower doses being less effective (Fig. 1a, Supplementary Fig. 1b). Although an inverted U-shaped drug response is common, a plausible explanation for the diminished effectiveness of higher doses is that WGE downregulates the day-time but not night-time locomotor activity of flies [49]. In mice, higher WGE doses have sleep-promoting effects by activating adenosine A_1/A_2A receptors in the

ventrolateral preoptic area [50]. Thus, dosage level is critical to the beneficial effects of GE in both PD models.

Gastrodin and 4-HBA are considered the principal active components in GE [37]. Although both compounds can cross the blood-brain barrier [38], the capability of gastrodin to do so is relatively poor compared to aglyconic 4-HBA due to the glucose moiety [51]. Gastrodin is quickly metabolized to 4-HBA and undetermined metabolites in the brain [52], perhaps explaining the lower effectiveness of gastrodin in G2019S flies. However, it is likely that the combination of gastrodin with other components in GE might exert optimal beneficial effects.

Expression of G2019S mutant protein impacts different clusters of dopaminergic neurons in the fly brain that are known for their connectivity and function. Activation of two specific mushroom body (MB)-projection dopaminergic neurons in the PPL1 cluster inhibits climbing performance [53]. Mutations in the circadian gene *Clock* (*Clk*) cause PPL1 dopaminergic neuron degeneration, accelerating impaired age-associated climbing ability [54]. Dopaminergic neurons in the PPL2 cluster extend processes to the calyx of the MB, which has been linked to climbing activity [53]. In contrast, PPM3 neurons project to the central complex, activation of which enhances locomotion [55]. A significant reduction in dopaminergic neurons in the PPM1/2 cluster was only found at week 4 when impaired locomotion of G2019S flies was prominent. In a PD fly model involving *SNCA* overexpression and *aux* knockdown, dopaminergic neurons in the PPM1/2 cluster were selectively degenerated and this phenotype was accompanied by impaired locomotion in relatively young adult flies [56]. We postulate that the age-dependent impaired locomotion displayed by G2019S flies could be caused by gradual and differential loss of dopaminergic neurons in

these clusters, thereby affecting different aspects of locomotion. However, further study is needed to test that hypothesis.

Expression of the G2019S mutant protein induces Lrrk2 auto- and hyper-phosphorylation, as well as protein accumulation, together enhancing cellular Lrrk2 activity and causing aberrant downstream signaling [4]. We have shown here that neuronal expression of Lrrk2-G2019S reduced Akt phosphorylation (Fig. 4a, b). Consistently, hyperactivated G2019S mutant protein impaired interaction with and phosphorylation of Akt, resulting in compromised signaling and accelerated neurodegeneration [57, 58]. However, WGE feeding restored downstream Akt signaling by suppressing G2019S mutant protein hyperactivation. Rab10, one of the best-characterized substrates for Lrrk2, mediates several of Lrrk2's cellular functions [41]. In *Drosophila*, Rab10 and Lrrk2-G2019S synergistically affect the activity of dopaminergic neurons, mediating deficits in movement [59, 60]. We have shown that WGE treatment downregulated levels of Lrrk2 accumulation and phosphorylated Rab10 (Fig. 3f-h), thus alleviating their synergistic toxicity. Several kinase inhibitors have been developed to block the kinase activity of Lrrk2, including of both wild-type Lrrk2 and the G2019S mutant, which could affect endogenous Lrrk2 activity [4]. Instead, WGE treatment modulates the phosphorylation status and protein level of the G2019S mutant but not those of wild-type Lrrk2. The new hydrogen bond created at the Ser^{2019} autophosphorylation site may provide a docking site for some chemicals in WGE, representing a possible explanatory mechanism that warrants further study [61].

The antioxidation and detoxification factor Nrf2 is a target of Akt activation. Nrf2 phosphorylation and HO-1 expression levels revealed that Nrf2 is inactivated in G2019S flies, but it was activated by WGE

treatment (Fig. 4c, d). Intriguingly, our genetic data indicate that Nrf2 primarily functions in the glia of G2019S flies, with Nrf2 depletion from glia eliminating the beneficial effects of WGE and glial Nrf2 activation partially substituting for WGE feeding (Fig. 5b). Cortical neurons express much lower levels of Nrf2 than astrocytes owing to hypo-acetylation and transcriptional repression of the *Nrf2* promoter [62]. Moreover, neurons express greater amounts of Cullin 3, the scaffold component of the E3 ubiquitin ligase that targets Nrf2 for proteasomal degradation [63]. Both those mechanisms render neuronal Nrf2 inert to activation. Nrf2 activation in astrocytes maintains neuronal integrity and function against oxidative insults in response to stress by supplying antioxidants such as glutathione and HO-1 [64, 65]. Previous study showed that 4-HBA triggers glia to secrete HO-1 via the Nrf2 pathway, protecting neurons from hydrogen peroxide in the primary culture [66]. In PD models in which wild-type or mutant α-synuclein is overexpressed, activation of neuronal Nrf2 [67, 68] or astrocytic Nrf2 [69] proved neuroprotective. By genetically manipulating the G2019S fly model, we have shown that WGE-induced Nrf2 activation in glia but not in neurons protects dopaminergic neurons from degeneration and ameliorates impaired locomotion.

Astrocyte-like and ensheathing glia are two major types of glia in the *Drosophila* nervous system, surrounding and also extending long processes into neuropils of the brain. These astrocyte-like glia exhibit a morphology and function similar to those of mammalian astrocytes, including reuptake of neurotransmitters and phagocytosis of neuronal debris [44, 70]. Ensheathing glia of varying morphologies encase axonal tracts and neuropils, regulating neuronal excitability and participating in phagocytosis and injury-induced inflammation [71, 72]. Thus, given their proximity to neurons and similar functions, it is not surprising that both types of glia collectively mediate the protective effects of WGE.

Communication between neurons and glia maintains homeostasis, yet also confers the disease state during neurodegeneration. In the *Drosophila* G2019S model, upregulation of the BMP ligand Gbb in dopaminergic neurons activates Mad/Smad signaling in glia, which promotes neuronal degeneration via a feedback mechanism [26]. Surprisingly, although the number of dopaminergic neurons in the fly brain is relatively small, the upregulated pMad signal spreads throughout the brain (Fig. 7b), suggesting that BMP can be disseminated over long distances. In PD patients, higher levels of transforming growth factor-β1 (TGF-β1) have been detected in the striatum and ventricular cerebrospinal fluid [73]. Thus, members of the TGF-β1 superfamily such as TGF-β1 and BMP signaling molecules may represent indicators of neuronal degeneration. Accordingly, disrupting the glia-to-neuron feedback mechanism may sustain neuronal survival. In glia, we found that WGE treatment downregulated the pMad levels that had been increased in the G2019S flies (Fig. 7a, b). Nrf2 activation in glia also suppressed the enhanced levels of pMad in mutant flies (Fig. 8b, c). Indeed, our genetic assays indicate that the Nrf2 and Mad pathways interact in the glia of G2019S flies. Thus, WGE exerts its beneficial effects by activating Nrf2 to antagonize the Mad activity that would otherwise contribute to the degeneration of dopaminergic neurons. As a transcriptional activator, Nrf2 induces expression of the inhibitory component Smad7 to form inactive Smad complexes [74] and the phosphatase subunit PPM1A to alter Smad2/3/4 phosphorylation and DNA binding [75]. Given that these components are conserved in *Drosophila*, Nrf2 may employ similar pathways to block Mad signaling in glia.

That glial Nrf2 activation protects neurons is evidenced by our observations of enhanced HO-1 expression (Fig. 4c) and increased numbers of dopaminergic neurons (Fig. 5e, f). These results support that

the role of Nrf2 in glia is to induce expression of antioxidation building blocks, such as phase-II detoxification enzymes, and to enhance inflammatory processes [76, 77]. In a model of fibrosis, TGF-β/Smad2/3 suppressed expression of the *ARE*-luciferase reporter and gluthathion [78]. Moreover, Nrf2 knockdown was shown to reduce expression of the antioxidative enzyme NAD(P)H quinone dehydrogenase 1 (NQO1), thereby elevating cellular oxidative stress and upregulating TGF-β/Smad targeted gene expression [79]. Hence, we propose that WGE promotes Nrf2 activation to antagonize the Smad signaling in glia that is induced by dopaminergic neuron-secreted BMP/Gbb signal during degeneration.

By employing a *G2019S* mouse model, we have also demonstrated that WGE rescues their locomotor coordination, suppresses their centrophobism, and recovers their numbers of dopaminergic neurons (Fig. 9a-d and Fig. 10a). Significantly, we found that activity of the TGF-β/Smad2/3 pathway was elevated in nigrostriatal brain lysates, and this activity was also suppressed by WGE treatment (Fig. 10e, g).

Conclusion

Collectively, these results from fly and mouse PD models indicate that the effectiveness of WGE is likely mediated through conserved Nrf2/Mad pathways. Our findings contribute to the mechanistic understanding of PD and provide potential therapeutic strategies that incorporate the traditional herbal medicine GE.

List of abbreviations

4-HBA: 4-hydroxybenzyl alcohol

Akt: Protein kinase B

ARE: Antioxidant response element

BMP: Bone morphogenetic proteins

cnc: Cap-n-collar

G2019S: Leucine-rich repeat kinase 2 with G2019S mutation

Gbb: Glass bottom boat

GDNF: Glia-derived neurotropic factor

GE: *Gastrodia elata* Blume

GSK3β: Glycogen synthase kinase 3β

HO-1: Heme oxygenase 1

Iba-1: Ionized calcium-binding adapter molecule 1

L-DOPA: Levodopa

LRRK2: Leucine-rich repeat kinase 2

Mad: Mothers against decapentaplegic

Nrf2: Nuclear factor-erythroid factor 2-related factor 2

nTg: Non-transgenic

PD: Parkinson's disease

PPL: Protocerebral posterior lateral

PPM: Protocerebral posterior medial

TCM: Traditional Chinese Medicine

TGF-β: Transforming growth factor-β

TH: Tyrosine hydroxylase

WGE: Water extract of *Gastrodia elata* Blume

Declarations

Ethics approval and consent to participate

All animal procedures were approved by the local ethics committee and the Institutional Animal Care and Use Committee (IACUC) of the National Taiwan University (IACUC approval no. 20180103).

Consent for publication

Not applicable.

Avaliability of data and materials

The authors declare that all data generated and/or analysed during the current study are available from the corresponding authors on reasonable request.

Competing interests

The authors declare that they have no competing interests.

Funding

This work was supported by grants from the Taiwan Ministry of Science and Technology (MOST-108-2311-B-001-039-MY3) to C.-T. C. S.P. and C.J.H.E. were supported by Parkinson's Disease Society of the United Kingdom (Parkinson’s UK), grant H1201.

Authors’ contributions

Y.-E.L., C.-H.L., L.-Y.S., and C.-T.C. designed the research. Y.-E.L., E.-P.H., and Y.-C.K. performed the experiments. S.P. and C.J.H.E. contributed new reagents. Y.-E.L., C.-H.L., E.-P.H., and Y.-C.K. analyzed the data. Y.-E.L., C.-H.L., L.-Y.S. and C.-T.C. drafted and revised the manuscript. All authors have read and approved the final manuscript.

Acknowledgements

We thank D. Bohmann (URMC), U. Heberlein (HHMI), S. J. Newfeld (ASU), T.-K. Sang (NTHU), Bloomington Stock Center, *Drosophila* Genomics Resource Center, Kyoto Stock Center and Taiwan Fly Core for providing fly stocks. We thank KO DA Pharmaceutical Co. Ltd. (Taoyuan, Taiwan) and Wuhan YC Fine Chemical Co. (Wuhan, China) for providing WGE and gastrodin, respectively.

References

1. Ray Chaudhuri K, Poewe W, Brooks D. Motor and nonmotor complications of levodopa: Phenomenology, risk factors, and imaging features. Mov Disord. 2018;33(6):909-19.

2. Houlden H, Singleton AB. The genetics and neuropathology of Parkinson's disease. Acta Neuropathol. 2012;124(3):325-38.

3. Martin I, Kim JW, Dawson VL, Dawson TM. LRRK2 pathobiology in Parkinson's disease. J Neurochem. 2014;131(5):554-65.

4. Sheng Z, Zhang S, Bustos D, Kleinheinz T, Le Pichon CE, Dominguez SL, et al. Ser1292 autophosphorylation is an indicator of LRRK2 kinase activity and contributes to the cellular effects of PD mutations. Sci Transl Med. 2012;4(164):164ra1.

5. Sofroniew MV, Vinters HV. Astrocytes: biology and pathology. Acta Neuropathol. 2010;119(1):7-35.

6. Lin LF, Doherty DH, Lile JD, Bektesh S, Collins F. GDNF: a glial cell line-derived neurotrophic factor for midbrain dopaminergic neurons. Science. 1993;260(5111):1130-2.

7. Kam TI, Hinkle JT, Dawson TM, Dawson VL. Microglia and astrocyte dysfunction in Parkinson's disease. Neurobiol Dis. 2020;144:105028.

8. Miklossy J, Arai T, Guo JP, Klegeris A, Yu S, McGeer EG, et al. LRRK2 expression in normal and pathologic human brain and in human cell lines. J Neuropathol Exp Neurol. 2006;65(10):953-63.

9. Slevin JT, Gash DM, Smith CD, Gerhardt GA, Kryscio R, Chebrolu H, et al. Unilateral intraputamenal glial cell line-derived neurotrophic factor in patients with Parkinson disease: response to 1 year of treatment and 1 year of withdrawal. J Neurosurg. 2007;106(4):614-20.

10. Whone A, Luz M, Boca M, Woolley M, Mooney L, Dharia S, et al. Randomized trial of intermittent intraputamenal glial cell line-derived neurotrophic factor in Parkinson's disease. Brain. 2019;142(3):512-25.

11. Henry AG, Aghamohammadzadeh S, Samaroo H, Chen Y, Mou K, Needle E, et al. Pathogenic LRRK2 mutations, through increased kinase activity, produce enlarged lysosomes with reduced degradative capacity and increase ATP13A2 expression. Hum Mol Genet. 2015;24(21):6013-28.

12. Moehle MS, Webber PJ, Tse T, Sukar N, Standaert DG, DeSilva TM, et al. LRRK2 inhibition attenuates microglial inflammatory responses. J Neurosci. 2012;32(5):1602-11.

13. Chen L, Feany MB. Alpha-synuclein phosphorylation controls neurotoxicity and inclusion formation in a *Drosophila* model of Parkinson disease. Nat Neurosci. 2005;8(5):657-63.

14. Liu Z, Wang X, Yu Y, Li X, Wang T, Jiang H, et al. A *Drosophila* model for LRRK2-linked parkinsonism. Proc Natl Acad Sci U S A. 2008;105(7):2693-8.

15. Clark IE, Dodson MW, Jiang C, Cao JH, Huh JR, Seol JH, et al. *Drosophila* pink1 is required for mitochondrial function and interacts genetically with parkin. Nature. 2006;441(7097):1162-6.

16. Lin CH, Tsai PI, Wu RM, Chien CT. LRRK2 G2019S mutation induces dendrite degeneration through mislocalization and phosphorylation of tau by recruiting autoactivated GSK3ss. J Neurosci. 2010;30(39):13138-49.

17. Kalinderi K, Bostantjopoulou S, Fidani L. The genetic background of Parkinson's disease: current progress and future prospects. Acta Neurol Scand. 2016;134(5):314-26.

18. Kim TH, Cho KH, Jung WS, Lee MS. Herbal medicines for Parkinson's disease: a systematic review of randomized controlled trials. PLoS One. 2012;7(5):e35695.

19. Li X, Zhang Y, Wang Y, Xu J, Xin P, Meng Y, et al. The mechanisms of Traditional Chinese Medicine underlying the prevention and treatment of Parkinson's disease. Front Pharmacol. 2017;8:634.

20. Chen PJ, Sheen LY. *Gastrodiae Rhizoma* (tian ma): a review of biological activity and antidepressant mechanisms. J Tradit Complement Med. 2011;1(1):31-40.

21. Jang JH, Son Y, Kang SS, Bae CS, Kim JC, Kim SH, et al. Neuropharmacological potential of *Gastrodia elata* Blume and its components. Evid Based Complement Alternat Med. 2015;2015:309261.

22. Yuan Y, Jin X, Liu J, Zhao X, Zhou J, Wang X, et al. The *Gastrodia elata* genome provides insights into plant adaptation to heterotrophy. Nat Commun. 2018;9(1):1615.

23. Lin YE, Lin SH, Chen WC, Ho CT, Lai YS, Panyod S, et al. Antidepressant-like effects of water extract of *Gastrodia elata* Blume in rats exposed to unpredictable chronic mild stress via modulation of monoamine regulatory pathways. J Ethnopharmacol. 2016;187:57-65.

24. Kumar H, Kim IS, More SV, Kim BW, Bahk YY, Choi DK. Gastrodin protects apoptotic dopaminergic neurons in a toxin-induced Parkinson's disease model. Evid Based Complement Alternat Med. 2013;2013:514095.

25. Doo AR, Kim SN, Hahm DH, Yoo HH, Park JY, Lee H, et al. *Gastrodia elata* Blume alleviates L-DOPA-induced dyskinesia by normalizing FosB and ERK activation in a 6-OHDA-lesioned Parkinson's disease mouse model. BMC Complement Altern Med. 2014;14:107.

26. Maksoud E, Liao EH, Haghighi AP. A neuron-glial trans-signaling cascade mediates LRRK2-induced neurodegeneration. Cell Rep. 2019;26(7):1774-86 e4.

27. Sang TK, Chang HY, Lawless GM, Ratnaparkhi A, Mee L, Ackerson LC, et al. A *Drosophila* model of mutant human parkin-induced toxicity demonstrates selective loss of dopaminergic neurons and dependence on cellular dopamine. J Neurosci. 2007;27(5):981-92.

28. Sykiotis GP, Bohmann D. Keap1/Nrf2 signaling regulates oxidative stress tolerance and lifespan in *Drosophila*. Dev Cell. 2008;14(1):76-85.

29. Bainton RJ, Tsai LT, Schwabe T, DeSalvo M, Gaul U, Heberlein U. *moody* encodes two GPCRs that regulate cocaine behaviors and blood-brain barrier permeability in *Drosophila*. Cell. 2005;123(1):145-56.

30. Takaesu NT, Hyman-Walsh C, Ye Y, Wisotzkey RG, Stinchfield MJ, O'Connor M B, et al. dSno facilitates baboon signaling in the *Drosophila* brain by switching the affinity of Medea away from Mad and toward dSmad2. Genetics. 2006;174(3):1299-313.

31. Lin YE, Chou ST, Lin SH, Lu KH, Panyod S, Lai YS, et al. Antidepressant-like effects of water extract of *Gastrodia elata* Blume on neurotrophic regulation in a chronic social defeat stress model. J Ethnopharmacol. 2018;215:132-9.

32. Madabattula ST, Strautman JC, Bysice AM, O'Sullivan JA, Androschuk A, Rosenfelt C, et al. Quantitative analysis of climbing defects in a *Drosophila* model of neurodegenerative disorders. J Vis Exp. 2015(100):e52741.

33. Chen AY, Wilburn P, Hao X, Tully T. Walking deficits and centrophobism in an alpha-synuclein fly model of Parkinson's disease. Genes Brain Behav. 2014;13(8):812-20.

34. Smith RB, Machamer JB, Kim NC, Hays TS, Marques G. Relay of retrograde synaptogenic signals through axonal transport of BMP receptors. J Cell Sci. 2012;125(Pt 16):3752-64.

35. Lin CH, Tsai PI, Lin HY, Hattori N, Funayama M, Jeon B, et al. Mitochondrial UQCRC1 mutations cause autosomal dominant parkinsonism with polyneuropathy. Brain. 2020;143(11):3352-73.

36. Angeby-Moller K, Berge OG, Hamers FP. Using the CatWalk method to assess weight-bearing and pain behaviour in walking rats with ankle joint monoarthritis induced by carrageenan: effects of morphine and rofecoxib. J Neurosci Methods. 2008;174(1):1-9.

37. Zhan HD, Zhou HY, Sui YP, Du XL, Wang WH, Dai L, et al. The rhizome of *Gastrodia elata* Blume - An ethnopharmacological review. J Ethnopharmacol. 2016;189:361-85.

38. Wu J, Wu B, Tang C, Zhao J. Analytical techniques and pharmacokinetics of *Gastrodia elata* Blume and its constituents. Molecules. 2017;22(7).

39. Mao Z, Davis RL. Eight different types of dopaminergic neurons innervate the *Drosophila* mushroom body neuropil: anatomical and physiological heterogeneity. Front Neural Circuits. 2009;3:5.

40. Price A, Manzoni C, Cookson MR, Lewis PA. The LRRK2 signalling system. Cell Tissue Res. 2018;373(1):39-50.

41. Karayel O, Tonelli F, Virreira Winter S, Geyer PE, Fan Y, Sammler EM, et al. Accurate MS-based Rab10 phosphorylation stoichiometry determination as readout for LRRK2 activity in Parkinson's disease. Mol Cell Proteomics. 2020;19(9):1546-60.

42. Lin CH, Lin HI, Chen ML, Lai TT, Cao LP, Farrer MJ, et al. Lovastatin protects neurite degeneration in LRRK2-G2019S parkinsonism through activating the Akt/Nrf pathway and inhibiting GSK3beta activity. Hum Mol Genet. 2016;25(10):1965-78.

43. Chatterjee N, Bohmann D. A versatile PhiC31 based reporter system for measuring AP-1 and Nrf2 signaling in *Drosophila* and in tissue culture. PLoS One. 2012;7(4):e34063.

44. Freeman MR. *Drosophila* central nervous system glia. Cold Spring Harb Perspect Biol. 2015;7(11):a020552.

45. Chou JS, Chen CY, Chen YL, Weng YH, Yeh TH, Lu CS, et al. (G2019S) LRRK2 causes early-phase dysfunction of SNpc dopaminergic neurons and impairment of corticostriatal long-term depression in the PD transgenic mouse. Neurobiol Dis. 2014;68:190-9.

46. Chen CY, Weng YH, Chien KY, Lin KJ, Yeh TH, Cheng YP, et al. (G2019S) LRRK2 activates MKK4-JNK pathway and causes degeneration of SN dopaminergic neurons in a transgenic mouse model of PD. Cell Death Differ. 2012;19(10):1623-33.

47. Grotewiel MS, Martin I, Bhandari P, Cook-Wiens E. Functional senescence in *Drosophila melanogaster*. Ageing Res Rev. 2005;4(3):372-97.

48. Kulisevsky J, Pagonabarraga J, Pascual-Sedano B, Garcia-Sanchez C, Gironell A, Trapecio Group S. Prevalence and correlates of neuropsychiatric symptoms in Parkinson's disease without dementia. Mov Disord. 2008;23(13):1889-96.

49. Jo K, Jeon S, Ahn CW, Han SH, Suh HJ. Changes in *Drosophila melanogaster* sleep-wake behavior due to lotus (*Nelumbo nucifera*) seed and Hwang Jeong (*Polygonatum sibiricum*) extracts. Prev Nutr Food Sci. 2017;22(4):293-9.

50. Zhang Y, Li M, Kang RX, Shi JG, Liu GT, Zhang JJ. NHBA isolated from *Gastrodia elata* exerts sedative and hypnotic effects in sodium pentobarbital-treated mice. Pharmacol Biochem Behav. 2012;102(3):450-7.

51. Lin LC, Chen YF, Tsai TR, Tsai TH. Analysis of brain distribution and biliary excretion of a nutrient supplement, gastrodin, in rat. Anal Chim Acta. 2007;590(2):173-9.

52. Lin LC, Chen YF, Lee WC, Wu YT, Tsai TH. Pharmacokinetics of gastrodin and its metabolite p-hydroxybenzyl alcohol in rat blood, brain and bile by microdialysis coupled to LC-MS/MS. J Pharm Biomed Anal. 2008;48(3):909-17.

53. Sun J, Xu AQ, Giraud J, Poppinga H, Riemensperger T, Fiala A, et al. Neural control of startle-induced locomotion by the mushroom bodies and associated neurons in *Drosophila*. Front Syst Neurosci. 2018;12:6.

54. Vaccaro A, Issa AR, Seugnet L, Birman S, Klarsfeld A. *Drosophila* Clock is required in brain pacemaker neurons to prevent premature locomotor aging independently of its circadian function. PLoS Genet. 2017;13(1):e1006507.

55. Kong EC, Woo K, Li H, Lebestky T, Mayer N, Sniffen MR, et al. A pair of dopamine neurons target the D1-like dopamine receptor DopR in the central complex to promote ethanol-stimulated locomotion in *Drosophila*. PLoS One. 2010;5(4):e9954.

56. Song L, He Y, Ou J, Zhao Y, Li R, Cheng J, et al. Auxilin underlies progressive locomotor deficits and dopaminergic neuron loss in a *Drosophila* model of Parkinson's disease. Cell Rep. 2017;18(5):1132-43.

57. Ohta E, Kawakami F, Kubo M, Obata F. LRRK2 directly phosphorylates Akt1 as a possible physiological substrate: impairment of the kinase activity by Parkinson's disease-associated mutations. FEBS Lett. 2011;585(14):2165-70.

58. Panagiotakopoulou V, Ivanyuk D, De Cicco S, Haq W, Arsic A, Yu C, et al. Interferon-gamma signaling synergizes with LRRK2 in neurons and microglia derived from human induced pluripotent stem cells. Nat Commun. 2020;11(1):5163.

59. Petridi S, Middleton CA, Ugbode C, Fellgett A, Covill L, Elliott CJH. In vivo visual screen for dopaminergic Rab <--> LRRK2-G2019S interactions in *Drosophila* discriminates Rab10 from Rab3. G3 (Bethesda). 2020;10(6):1903-14.

60. Fellgett A, Middleton CA, Munns J, Ugbode C, Jaciuch D, Wilson L, et al. Multiple pathways of LRRK2-G2019S/Rab10 interaction in dopaminergic neurons. J Parkinsons Dis. 2021;10.3233/jpd-202421.

61. Lang CA, Ray SS, Liu M, Singh AK, Cuny GD. Discovery of LRRK2 inhibitors using sequential in silico joint pharmacophore space (JPS) and ensemble docking. Bioorg Med Chem Lett. 2015;25(13):2713-9.

62. Bell KF, Al-Mubarak B, Martel MA, McKay S, Wheelan N, Hasel P, et al. Neuronal development is promoted by weakened intrinsic antioxidant defences due to epigenetic repression of Nrf2. Nat Commun. 2015;6:7066.

63. Jimenez-Blasco D, Santofimia-Castano P, Gonzalez A, Almeida A, Bolanos JP. Astrocyte NMDA receptors' activity sustains neuronal survival through a Cdk5-Nrf2 pathway. Cell Death Differ. 2015;22(11):1877-89.

64. Kraft AD, Johnson DA, Johnson JA. Nuclear factor E2-related factor 2-dependent antioxidant response element activation by tert-butylhydroquinone and sulforaphane occurring preferentially in astrocytes conditions neurons against oxidative insult. J Neurosci. 2004;24(5):1101-12.

65. Vargas MR, Johnson JA. The Nrf2-ARE cytoprotective pathway in astrocytes. Expert Rev Mol Med. 2009;11:e17.

66. Luo L, Kim SW, Lee HK, Kim ID, Lee H, Lee JK. Anti-oxidative effects of 4-hydroxybenzyl alcohol in astrocytes confer protective effects in autocrine and paracrine manners. PLoS One. 2017;12(5):e0177322.

67. Barone MC, Sykiotis GP, Bohmann D. Genetic activation of Nrf2 signaling is sufficient to ameliorate neurodegenerative phenotypes in a *Drosophila* model of Parkinson's disease. Dis Model Mech. 2011;4(5):701-7.

68. Skibinski G, Hwang V, Ando DM, Daub A, Lee AK, Ravisankar A, et al. Nrf2 mitigates LRRK2- and alpha-synuclein-induced neurodegeneration by modulating proteostasis. Proc Natl Acad Sci U S A. 2017;114(5):1165-70.

69. Gan L, Vargas MR, Johnson DA, Johnson JA. Astrocyte-specific overexpression of Nrf2 delays motor pathology and synuclein aggregation throughout the CNS in the alpha-synuclein mutant (A53T) mouse model. J Neurosci. 2012;32(49):17775-87.

70. Tasdemir-Yilmaz OE, Freeman MR. Astrocytes engage unique molecular programs to engulf pruned neuronal debris from distinct subsets of neurons. Genes Dev. 2014;28(1):20-33.

71. Otto N, Marelja Z, Schoofs A, Kranenburg H, Bittern J, Yildirim K, et al. The sulfite oxidase Shopper controls neuronal activity by regulating glutamate homeostasis in *Drosophila* ensheathing glia. Nat Commun. 2018;9(1):3514.

72. Doherty J, Logan MA, Tasdemir OE, Freeman MR. Ensheathing glia function as phagocytes in the adult *Drosophila* brain. J Neurosci. 2009;29(15):4768-81.

73. Vawter MP, Dillon-Carter O, Tourtellotte WW, Carvey P, Freed WJ. TGFbeta1 and TGFbeta2 concentrations are elevated in Parkinson's disease in ventricular cerebrospinal fluid. Exp Neurol. 1996;142(2):313-22.

74. Song MK, Lee JH, Ryoo IG, Lee SH, Ku SK, Kwak MK. Bardoxolone ameliorates TGF-beta1-associated renal fibrosis through Nrf2/Smad7 elevation. Free Radic Biol Med. 2019;138:33-42.

75. Lin X, Duan X, Liang YY, Su Y, Wrighton KH, Long J, et al. PPM1A functions as a Smad phosphatase to terminate TGFbeta signaling. Cell. 2006;125(5):915-28.

76. Hirrlinger J, Dringen R. The cytosolic redox state of astrocytes: Maintenance, regulation and functional implications for metabolite trafficking. Brain Res Rev. 2010;63(1-2):177-88.

77. Rojo AI, Innamorato NG, Martin-Moreno AM, De Ceballos ML, Yamamoto M, Cuadrado A. Nrf2 regulates microglial dynamics and neuroinflammation in experimental Parkinson's disease. Glia. 2010;58(5):588-98.

78. Ryoo IG, Ha H, Kwak MK. Inhibitory role of the KEAP1-NRF2 pathway in TGFbeta1-stimulated renal epithelial transition to fibroblastic cells: a modulatory effect on SMAD signaling. PLoS One. 2014;9(4):e93265.

79. Prestigiacomo V, Suter-Dick L. Nrf2 protects stellate cells from Smad-dependent cell activation. PLoS One. 2018;13(7):e0201044.

Figure legends

Fig. 1 WGE treatment rescues the diminished locomotion of *Ddc>G2019S* mutant flies.

a-c Climbing activities of *Ddc>G2019S* flies fed on food supplemented with 0.1%, 0.5% or 1.0% WGE (**a**), 0.1 or 1.0 mM gastrodin (**b**), and 0.1 or 1.0 mM 4-HBA (**c**). Controls are *Ddc>Lrrk* and *Ddc>G2019S* flies fed regular food. Bar graphs show the percentages of flies (mean ± SEM, N = 6) that climbed above 8 cm within 10 sec. **d** Five-minute walking tracks pooled from eight flies each of the *Ddc>Lrrk*, *Ddc>G2019S*, and *Ddc>G2019S* + 0.1% WGE groups at week 4. Bar graph at right summarizes their walking distances (mean ± SEM, N = 8). One-way analysis of variance (ANOVA) with Tukey's post-hoc multiple comparison test: * $p < 0.05$, ** $p < 0.01$, and *** $p < 0.001$, ns, not significant.

Fig. 2 WGE prevents loss of dopaminergic neurons in *Ddc>G2019S* flies.

a Representative adult brain images showing TH-positive dopaminergic neurons in the PPL1 cluster of 2-, 4-, and 6-week-old flies of the *Ddc>Lrrk2*, *Ddc>G2019S*, and 0.1% WGE-fed *Ddc>G2019S* groups. Scale bar: 10 μm. **b** Average numbers (mean ± SEM, N = 5) of TH-positive dopaminergic neurons in the PPL1, PPM1/2, PPL2, and PPL3 clusters per brain hemisphere. One-way ANOVA with Tukey's post-hoc multiple comparison test: * $p < 0.05$, ** $p < 0.01$, *** $p < 0.001$, ns, not significant.

Fig. 3 WGE modulates Lrrk2 accumulation and hyperactivation in *elav>G2019S* flies.

a Representative immunoblots of 3-day-old adult brain lysates showing expression levels of Lrrk2, pLrrk2 (phosphoryled at Ser^{1292}), Akt, and pAkt (phosphorylated at Ser^{505}) in *elav>Lrrk2* and *elav>G2019S* flies. **b**,

c Quantifications (mean ± SEM, N = 3) of Lrrk2 and pLrrk2/Lrrk2 (**b**), and Akt and pAkt/Akt (**c**). **d** Representative immunoblots of 2- and 4-week-old adult brain lysates showing Lrrk2 levels in the fly groups *elav>Lrrk2*, *elav>G2019S*, and *elav>G2019S* fed with 0.1% WGE. **e** Quantification of Lrrk2 levels in 2- and 4-week-old adult brains (mean ± SEM, N = 3). **f** Representative immunoblots of 4-week-old adult brain lysates showing expression levels of Lrrk2, pLrrk2, Rab10 and pRab10 (phosphorylated at Thr^{73}). **g**, **h** Quantification (mean ± SEM, N = 3) of levels of Lrrk2 and pLrrk2/Lrrk2 (**g**), and of Rab10 and pRab10/Rab10 (**h**). One-way ANOVA with Tukey's post-hoc multiple comparison test: * $p < 0.05$, ** $p < 0.01$, ns, not significant.

Fig. 4 WGE activates the Akt-Nrf2 pathway in *elav>G2019S* flies.

a Representative immunoblots of 2- and 4-week-old adult brain lysates showing levels of Akt and pAkt in brain extracts of *elav>Lrrk2*, *elav>G2019S*, and WGE-fed *elav>G2019S* flies. **b** Quantification (mean ± SEM, N = 3) of pAkt/Akt levels in 2- and 4-week-old adult brains. **c** Representative immunoblots of 4-week-old adult brain lysates showing levels of Nrf2, pNrf2 (phosphorylated at Ser^{40}), GSK3β, pGSK3β (phosphorylated at Ser^{9}), and HO-1 in *elav>Lrrk2*, *elav>G2019S*, and WGE-fed *elav>G2019S* flies. GADPH acted as a loading control in (**a**, **c**). **d** Quantification (mean ± SEM, N = 3) of relative protein levels to respective Nrf2, GSK3β, and HO-1. One-way ANOVA with Tukey's post-hoc multiple comparison test (relative to *elav>G2019S*): * $p < 0.05$, ** $p < 0.01$, *** $p < 0.001$, ns, not significant.

Fig. 5 Activation of Nrf2 in glia rescues locomotion defects in *Ddc>G2019S* flies.

a, **b** Requirement of Nrf2 in glia but not neurons for WGE-improved *Ddc>G2019S* climbing activity. **a** Climbing success rates of flies in which *Ddc-GAL4* drives co-expression of *Lrrk2-G2019S* and *mCD8-GFP*, *cncC-FL2* or *cnc-RNAi*. As a control line, *Ddc-GAL4* drives co-expression of *Lrrk2* and *mCD8-GFP*. **b** Climbing success rates of flies in which *Ddc-LexA* drives wild-type *Lrrk2* or *Lrrk2-G2019S* expression and *repo-GAL4* drives *cncC-FL2* or *cnc-RNAi* expression (mean ± SEM, N = 6 for **a** and **b**). WGE was added to food at a concentration of 0.1% (w/w). **c**, **d** WGE treatment activates glial Nrf2 signals. ARE-GFP (green) and glial Repo (red) in whole-mount adult brains without (**c**) or with 0.1% WGE treatment (**d**) for 5 days. Phalloidin (in blue) reveals brain structures. White arrowheads indicate GFP signals. Scale bar: 50 μm. Dotted boxes are enhanced views and shown as separate channels at right. **e** Adult brain images showing TH-positive dopaminergic neurons in the PPL1 clusters of 6-week-old *Ddc-LexA>Lrrk2* or *Ddc-LexA>G2019S* flies with *repo-GAL4* control or *repo-GAL4*-driven *cncC-FL2* or *cnc-RNAi* expression. Scale bar: 10 μm. **f** Average numbers (mean ± SEM, N = 5) of TH-positive dopaminergic neurons in PPL1 clusters per brain hemisphere are shown. One-way ANOVA with Tukey's post-hoc multiple comparison test (relative to *Ddc>G2019S* (**a**) or *Ddc-LexA>G2019S; repo-GAL4* (**b**, **f**)): ** $p < 0.01$, *** $p < 0.001$, ns, not significant.

Fig. 6 Nrf2 in astrocyte-like and ensheathing glia mediates the effect of WGE treatment in *Ddc>G2019S* flies.

a Nrf2 knockdown in astrocyte-like and ensheathing glia abolishes the improved locomotion elicited by WGE treatment in *Ddc>G2019S* flies. Composite bar graph shows climbing success rates for 6-week-old

Ddc-LexA>G2019S flies with *cnc-RNAi* driven by *repo-GAL4* in all glia, *alrm-GAL4* in astrocyte-like glia, *np2222* in cortex glia, *np6293* in perineurial glia, *R56F03* in ensheathing glia, and *moody-GAL4* in subperineurial glia. **b** Composite bar graph shows climbing success rates (mean ± SEM, N = 6) for 6-week-old *Ddc-LexA>G2019S* flies with overexpression of Nrf2 in astrocyte-like glia (*alrm>cncC-FL2*) or ensheathing glia (*R56F03>cncC-FL2*). One-way ANOVA and Tukey's post-hoc multiple comparison test (relative to *Ddc-LexA>G2019S; GAL4>cnc-RNAi* (**a**) or *Ddc-LexA>G2019S*; *GAL4* (**b**)): * $p < 0.05$, *** $p < 0.001$, ns, not significant. **c**, **e** Representative images showing expression of *ARE-GFP* in astrocyte-like glia (*alrm>mCherry*) (**c**) and ensheathing glia (*R56F03>mCherry*) (**e**), together with TH-positive dopaminergic neurons in the PPL1 clusters of *Ddc-LexA>Lrrk2*, *Ddc-LexA>G2019S*, or WGE (0.1% w/w)-fed *Ddc-LexA>G2019S* flies. Bar: 5 μm. GFP channels in the dashed boxes are shown as enhanced views in the lower panel, with glial signals labeled by dashed lines. **d**, **f** Quantifications (mean ± SEM, n > 25 for each genotype) of GFP intensities in astrocyte-like glia (**d**) or ensheathing glia (**f**). GFP intensities in glia have been outlined manually using the mCherry-positive signals. One-way ANOVA and Tukey's post-hoc multiple comparison test (relative to *Ddc-LexA>G2019S; alrm>mCherry* (**d**) or *Ddc-LexA>G2019S; R56F03>mCherry* (**f**)): * $p < 0.05$, *** $p < 0.001$, ns, not significant.

Fig. 7 WGE down-regulates G2019S-induced BMP/Mad signaling.

a Representative images of glial pMad staining in the adult PPL1 clusters of *Ddc>Lrrk2*, *Ddc>G2019S*, and WGE-fed *Ddc>G2019S* flies. White arrows indicate pMad signals co-localized with Repo, with single channels for pMad signals shown as insets. Bar: 10 μm. **b** Quantification (mean ± SEM, n > 60 for each

genotype) of pMad signals normalized to Repo levels in glia of the indicated genotypes. One-way ANOVA and Tukey's post-hoc multiple comparison test (relative to *Ddc>G2019S*): *** $p < 0.001$. **c**, **d** Climbing success rates (mean ± SEM, N = 10) at weeks 1-4 demonstrating that WGE treatment rescues locomotion deficits induced by glial overexpression of *Mad* (**c**) or tkv^{Q253D} (**d**) in *Tub-GAL80^{ts}; repo-GAL4* flies. One-way ANOVA and Tukey's post-hoc multiple comparison test (relative to *repo>Mad* or *repo>*tkv^{Q253D}): ** $p < 0.01$, *** $p < 0.001$. **e**, **g** Representative images of 4-week-old adult brain showing TH staining of the PPL1 clusters of *Tub-GAL80^{ts}; repo-GAL4*, *Tub-GAL80^{ts}; repo>Mad*, and WGE-fed *Tub-GAL80^{ts}; repo>Mad* flies (**e**), and *Tub-GAL80^{ts}; repo-GAL4*, *Tub-GAL80^{ts}; repo>*tkv^{Q253D}, and WGE-fed *Tub-GAL80^{ts}; repo>*tkv^{Q253D} flies (**g**). Bars: 12.5 μm. **f**, **h** Bar graphs show mean ± SEM (N = 5) of TH-positive dopaminergic neurons in the PPL1 clusters of 4-week-old flies. One-way ANOVA and Tukey's post-hoc multiple comparison test (relative to *Tub-GAL80^{ts}; repo>Mad* (**f**) or *Tub-GAL80^{ts}; repo>*tkv^{Q253D} (**h**)): *** $p < 0.001$.

Fig. 8 Nrf2 antagonizes BMP/Mad signaling in glia.

a Heterozygosity of *Mad* suppresses G2019S mutation-induced locomotion impairment in a negative geotaxis assay. Bar graph shows percentages (mean ± SEM, N = 6) of 6-week-old flies that climbed above 8 cm within 10 sec. One-way ANOVA and Tukey's post-hoc multiple comparison test: * $p < 0.05$, ** $p < 0.01$, *** $p < 0.001$, ns, not significant. **b** Representative images of pMad staining in the adult brains of *Ddc-LexA>Lrrk2* or *Ddc-LexA>G2019S* flies in which *repo-GAL4* drives expression of *cncC-FL2* or *cnc-RNAi*. Impact of WGE treatment is shown in the rightmost panels. Arrows indicate pMad and Repo

dual-positive cells. Insets are enlarged images of the dashed boxes, and dashed lines encompass Repo-positive cells. Bar: 20 μm. **c** Quantification of the ratio of pMad to Repo (mean ± SEM, N > 40). One-way ANOVA and Tukey's post-hoc multiple comparison test: *** $p < 0.001$, ns, not significant. **d** Images show pan-glial *ARE-GFP* expression (*repo>mCherry*) in *Ddc-LexA>Lrrk2*, *Ddc-LexA>G2019S*, and *Ddc-LexA>G2019S*, *Mad*$^{+/-}$ fly brains. GFP channels within the dashed boxes are shown as enhanced views in the inset, with glial signals outlined by dashed lines. Bar: 20 μm. **e** Quantification for GFP expression levels (mean ± SEM, n > 13). One-way ANOVA and Tukey's post-hoc multiple comparison test: * $p < 0.05$, *** $p < 0.001$.

Fig. 9 WGE treatment rescues impaired locomotion of *G2019S* mice.

a Video-tracked paths for nTg, *G2019S* and WGE-fed *G2019S* mice (8.5 and 11.5 months old) during the open-field test. **b** Quantification of total distance (meters, m), average velocity (centimeters per sec, cm/s), and percentage moving time for 8.5, 9.5, 10.5 and 11.5 months old mice. **c** Captured and converted images of single stance for each paw of 11.5-month-old nTg, *G2019S* and WGE-fed *G2019S* mice in a catwalk analysis. **d** Quantification of stride length for each paw of 8.5- and 11.5-month-old mice. Data in (**b**, **d**) are presented as mean ± SEM (nTg; N = 5, *G2019S*; N = 6, WGE-fed *G2019S*; N = 6). One-way ANOVA and Tukey's post-hoc multiple comparison test: * $p < 0.05$, ** $p < 0.01$, *** $p < 0.001$, ns, not significant. RF – right front; RH – right hind; LF – left front; LH – left hind.

Fig. 10 WGE prevents dopaminergic neuron loss, microglial activation, and phosphorylation of

Lrrk2, Smad2, and Smad3.

a, **c** Representative images showing TH-positive dopaminergic neurons (**a**) or Iba-1-positive microglia (**c**) in the substantia nigra of 11.5-month-old nTg, *G2019S* and WGE-fed *G2019S* mice. Bars: 100 μm in (**a**) and 50 μm in (**c**). **b**, **d** Quantification of numbers of TH-positive (**b**) or Iba-1-positive cells (**d**) relative to DAPI cells. **e** Representative immunoblots of nigrostriatal lysates prepared from 11.5-month-old nTg, *G2019S* and WGE-fed *G2019S* mice reveal expression levels of Lrrk2, pLrrk2 (Ser^{1292}), Smad2, pSmad2 (Ser^{465} and Ser^{467}), Smad3, and pSmad3 (Ser^{423} and Ser^{425}). Actin acted as a loading control. **f-g** Quantifications of Lrrk2 and pLrrk2/Lrrk2 (**f**), as well as pSmad2/Smad2 and pSmad3/Smad3 (**g**). Data in (**b**, **d**, **f**, **g**) are presented as mean ± SEM (N = 3). One-way ANOVA and Tukey's post-hoc multiple comparison test: * $p < 0.05$, ** $p < 0.01$, *** $p < 0.001$, ns, not significant.

Supplementary Information

Additional file 1

Supplementary figures 1-6.pdf

Supplementary Figure 1. Climbing activity assay of *Ddc>mCD8-GFP* and *Ddc>Lrrk2* flies (corresponding to Fig. 1).

Supplementary Figure 2. WGE treatment prevents dopaminergic neuron loss in *Ddc>G2019S* flies (corresponding to Fig. 2).

Supplementary Figure 3. WGE specifically modulates Lrrk2 accumulation and hyperactivation in *elav>G2019S* but not *elav>Lrrk2* flies (corresponding to Fig. 3).

Supplementary Figure 4. WGE rescues the locomotion defect displayed by *Ddc-LexA>G2019S* flies (corresponding to Fig. 5).

Supplementary Figure 5. Lrrk2 and pLrrk2 levels are maintained upon glial Nrf2 overexpression (corresponding to Fig. 6).

Supplementary Figure 6. *Mad* heterozygosity rescues the impaired locomotion of *Ddc>G2019S* flies (corresponding to Fig. 7).

Fig. 1

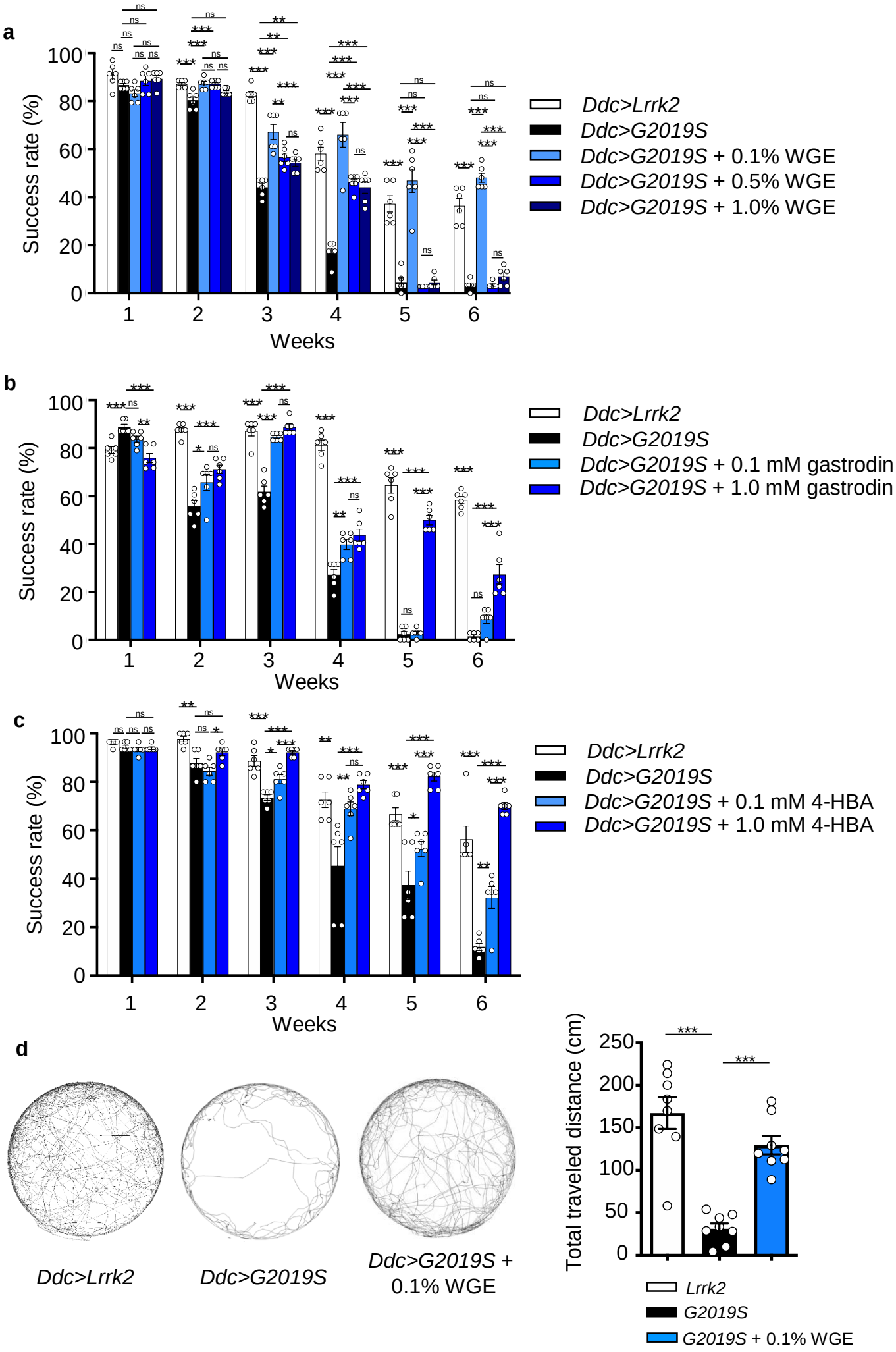
a
Success rate (%)
Weeks
Ddc>Lrrk2
Ddc>G2019S
Ddc>G2019S + 0.1% WGE
Ddc>G2019S + 0.5% WGE
Ddc>G2019S + 1.0% WGE
b
Success rate (%)
Weeks
Ddc>Lrrk2
Ddc>G2019S
Ddc>G2019S + 0.1 mM gastrodin
Ddc>G2019S + 1.0 mM gastrodin
c
Success rate (%)
Weeks
Ddc>Lrrk2
Ddc>G2019S
Ddc>G2019S + 0.1 mM 4-HBA
Ddc>G2019S + 1.0 mM 4-HBA
d
Ddc>Lrrk2
Ddc>G2019S
Ddc>G2019S + 0.1% WGE
Total traveled distance (cm)
Lrrk2
G2019S
G2019S + 0.1% WGE

Fig. 2

a

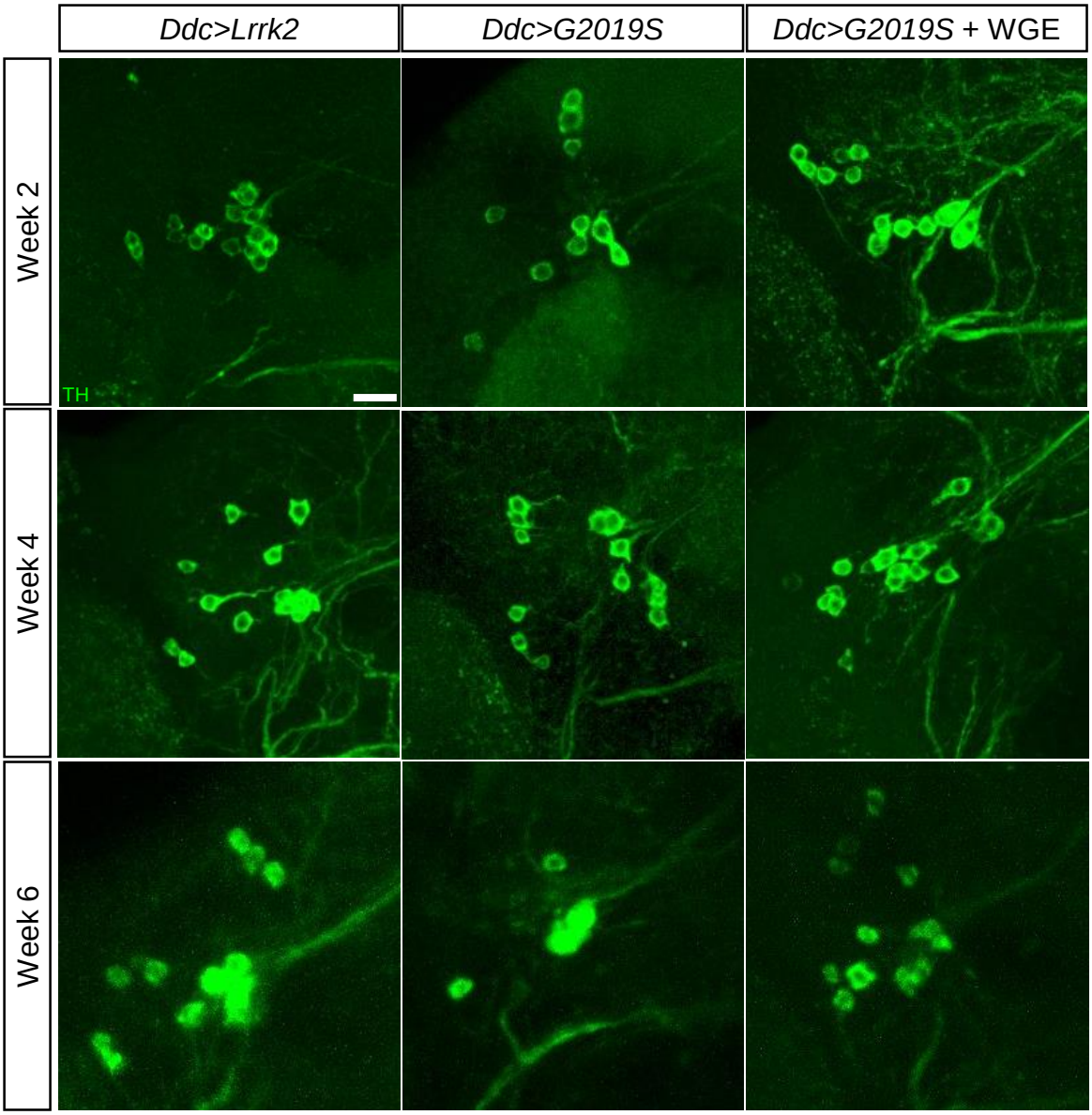
Ddc>Lrrk2
Ddc>G2019S
Ddc>G2019S + WGE
Week 2
Week 4
Week 6
TH

b

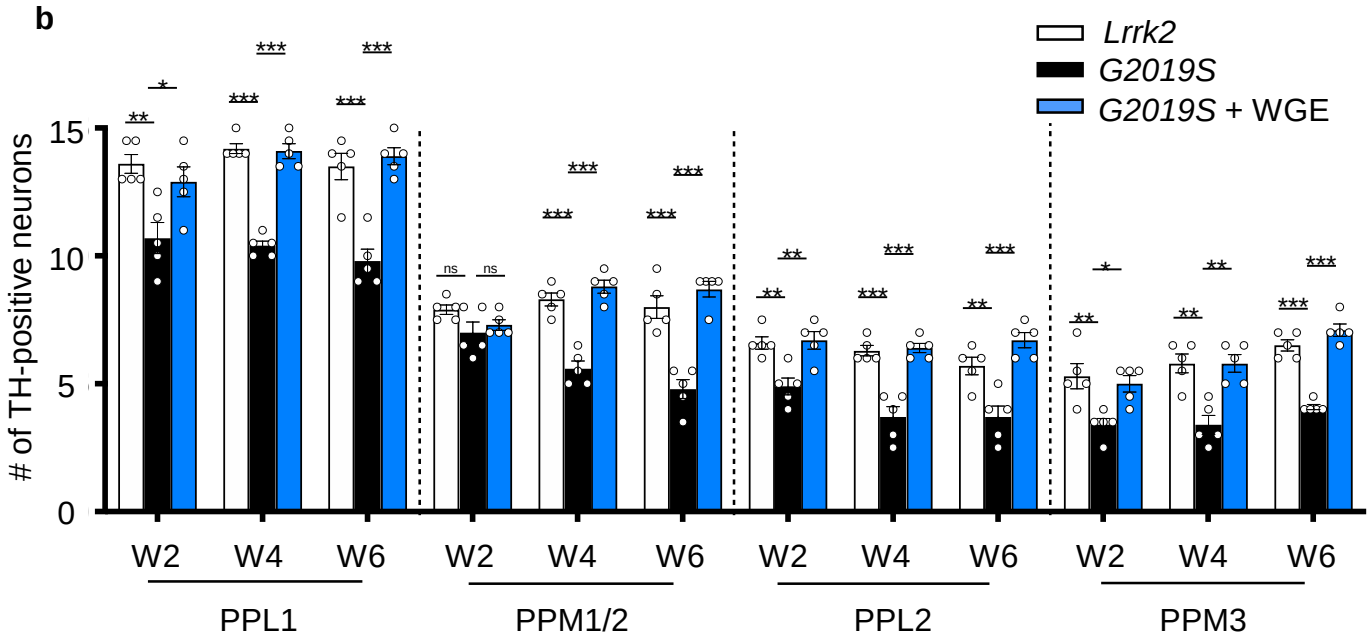
Lrrk2
G2019S
G2019S + WGE
# of TH-positive neurons
0
5
10
15
W2
W4
W6
PPL1
PPM1/2
PPL2
PPM3
ns
*
**
***

Fig. 3

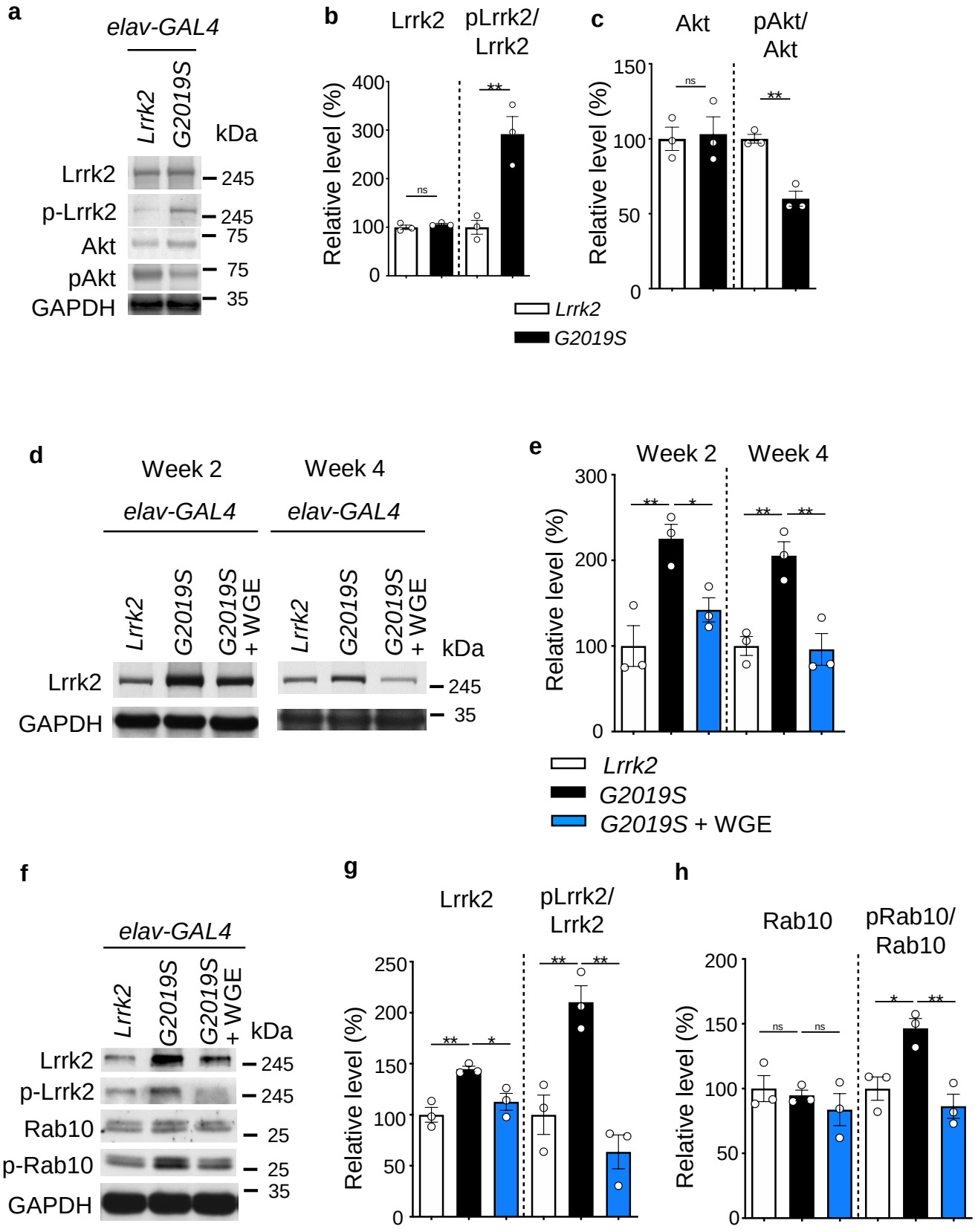
a
elav-GAL4
Lrrk2
G2019S
kDa
Lrrk2
p-Lrrk2
Akt
pAkt
GAPDH
245
245
75
75
35
b
Lrrk2
pLrrk2/ Lrrk2
Relative level (%)
400
300
200
100
0
ns
**
c
Akt
pAkt/ Akt
Relative level (%)
150
100
50
0
ns
**
Lrrk2
G2019S
d
Week 2
Week 4
elav-GAL4
elav-GAL4
Lrrk2
G2019S
G2019S + WGE
Lrrk2
G2019S
G2019S + WGE
kDa
Lrrk2
GAPDH
245
35
e
Week 2
Week 4
Relative level (%)
300
200
100
0
**
*
**
**
Lrrk2
G2019S
G2019S + WGE
f
elav-GAL4
Lrrk2
G2019S
G2019S + WGE
kDa
Lrrk2
p-Lrrk2
Rab10
p-Rab10
GAPDH
245
245
25
25
35
g
Lrrk2
pLrrk2/ Lrrk2
Relative level (%)
250
200
150
100
50
0
**
*
**
**
h
Rab10
pRab10/ Rab10
Relative level (%)
200
150
100
50
0
ns
ns
*
**

Fig. 4

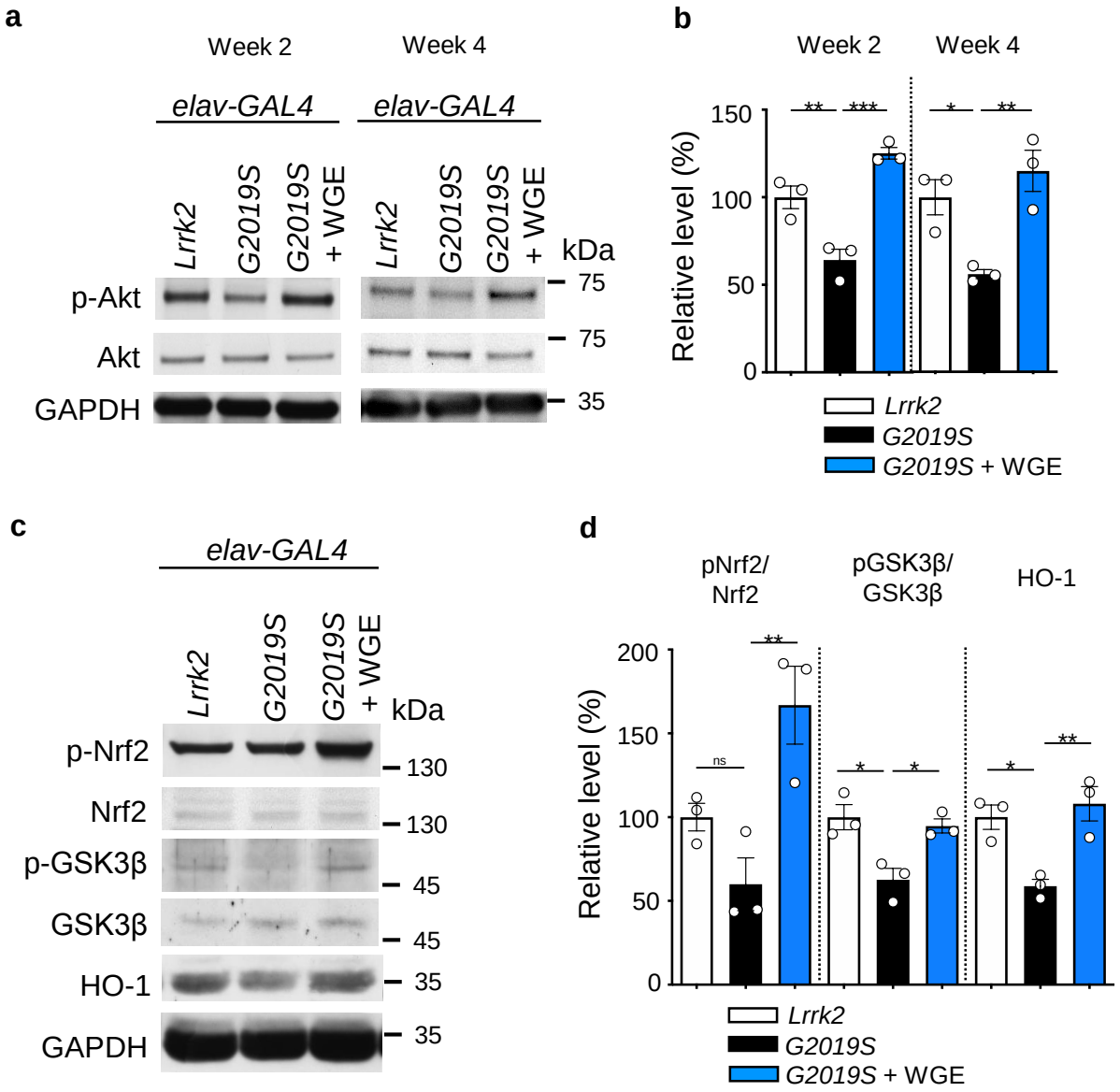
a
Week 2
Week 4
elav-GAL4
elav-GAL4
Lrrk2
G2019S
G2019S + WGE
Lrrk2
G2019S
G2019S + WGE
kDa
p-Akt
Akt
GAPDH
75
75
35
b
Week 2
Week 4
Relative level (%)
150
100
50
0
**
***
*
**
Lrrk2
G2019S
G2019S + WGE
c
elav-GAL4
Lrrk2
G2019S
G2019S + WGE
kDa
p-Nrf2
Nrf2
p-GSK3β
GSK3β
HO-1
GAPDH
130
130
45
45
35
35
d
pNrf2/ Nrf2
pGSK3β/ GSK3β
HO-1
Relative level (%)
200
150
100
50
0
ns
**
*
*
*
**
Lrrk2
G2019S
G2019S + WGE

Fig. 5

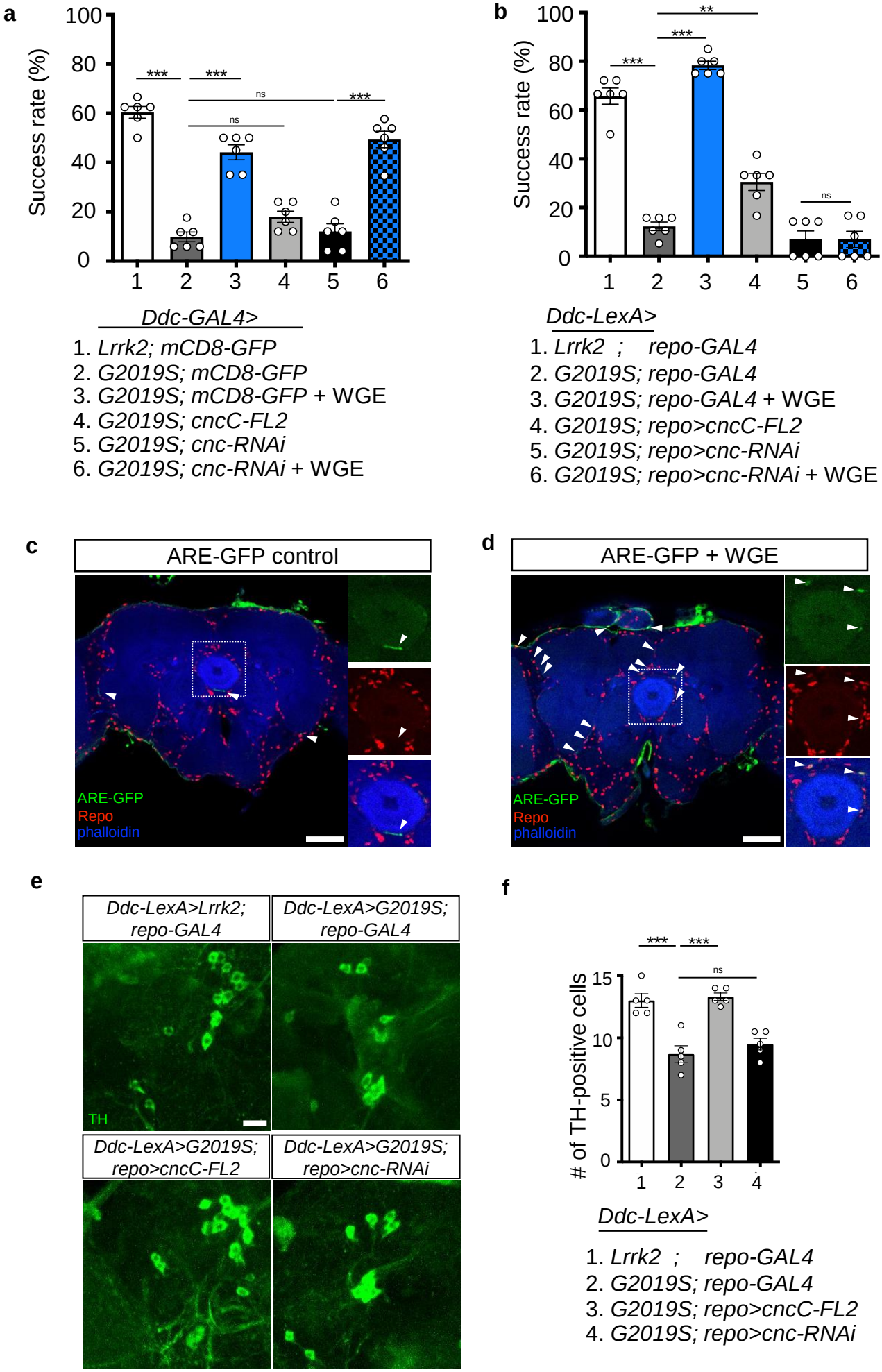
a
Success rate (%)
100
80
60
40
20
0
***
***
ns
ns
***
1
2
3
4
5
6
Ddc-GAL4>
1. Lrrk2; mCD8-GFP
2. G2019S; mCD8-GFP
3. G2019S; mCD8-GFP + WGE
4. G2019S; cncC-FL2
5. G2019S; cnc-RNAi
6. G2019S; cnc-RNAi + WGE
b
Success rate (%)
ns
**
***
***
ns
Ddc-LexA>
1. Lrrk2 ; repo-GAL4
2. G2019S; repo-GAL4
3. G2019S; repo-GAL4 + WGE
4. G2019S; repo>cncC-FL2
5. G2019S; repo>cnc-RNAi
6. G2019S; repo>cnc-RNAi + WGE
c
ARE-GFP control
ARE-GFP
Repo
phalloidin
d
ARE-GFP + WGE
ARE-GFP
Repo
phalloidin
e
Ddc-LexA>Lrrk2; repo-GAL4
Ddc-LexA>G2019S; repo-GAL4
TH
Ddc-LexA>G2019S; repo>cncC-FL2
Ddc-LexA>G2019S; repo>cnc-RNAi
f
# of TH-positive cells
15
10
5
0
***
***
ns
1
2
3
4
Ddc-LexA>
1. Lrrk2 ; repo-GAL4
2. G2019S; repo-GAL4
3. G2019S; repo>cncC-FL2
4. G2019S; repo>cnc-RNAi

Fig. 6

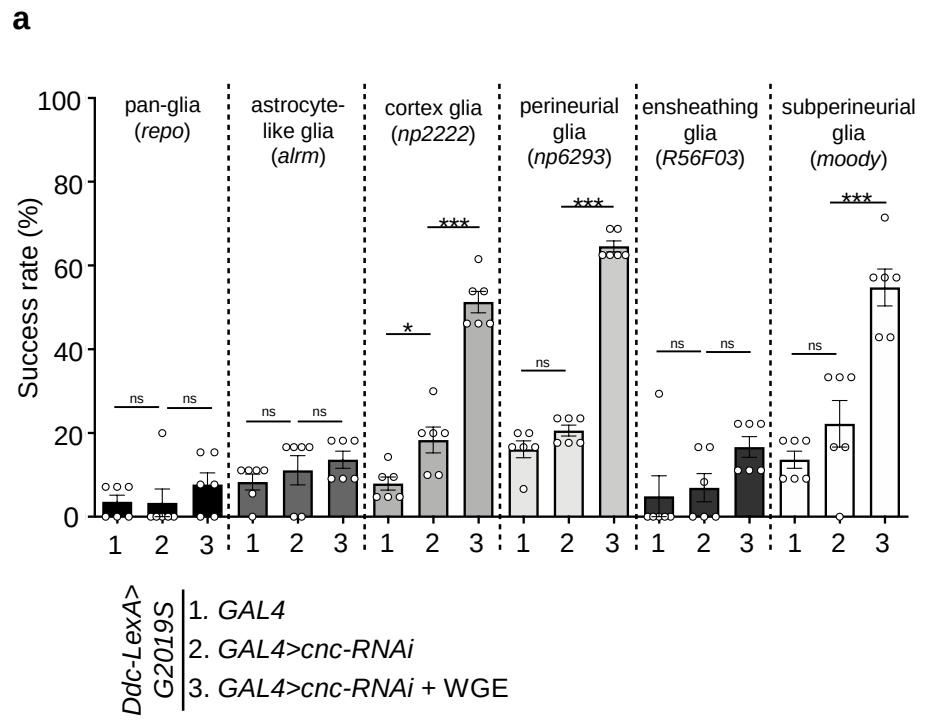
a
Success rate (%)
100
80
60
40
20
0
pan-glia (repo)
astrocyte-like glia (alrm)
cortex glia (np2222)
perineurial glia (np6293)
ensheathing glia (R56F03)
subperineurial glia (moody)
ns
*
***
1 2 3
Ddc-LexA> G2019S
1. GAL4
2. GAL4>cnc-RNAi
3. GAL4>cnc-RNAi + WGE

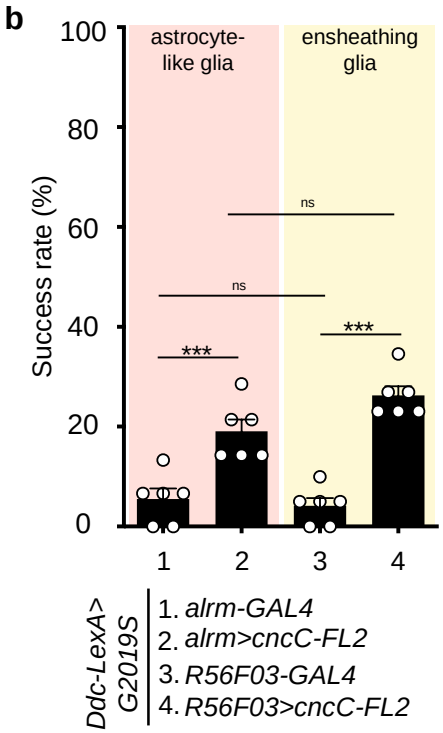
b
Success rate (%)
100
80
60
40
20
0
astrocyte-like glia
ensheathing glia
ns
***
1 2 3 4
Ddc-LexA> G2019S
1. alrm-GAL4
2. alrm>cncC-FL2
3. R56F03-GAL4
4. R56F03>cncC-FL2

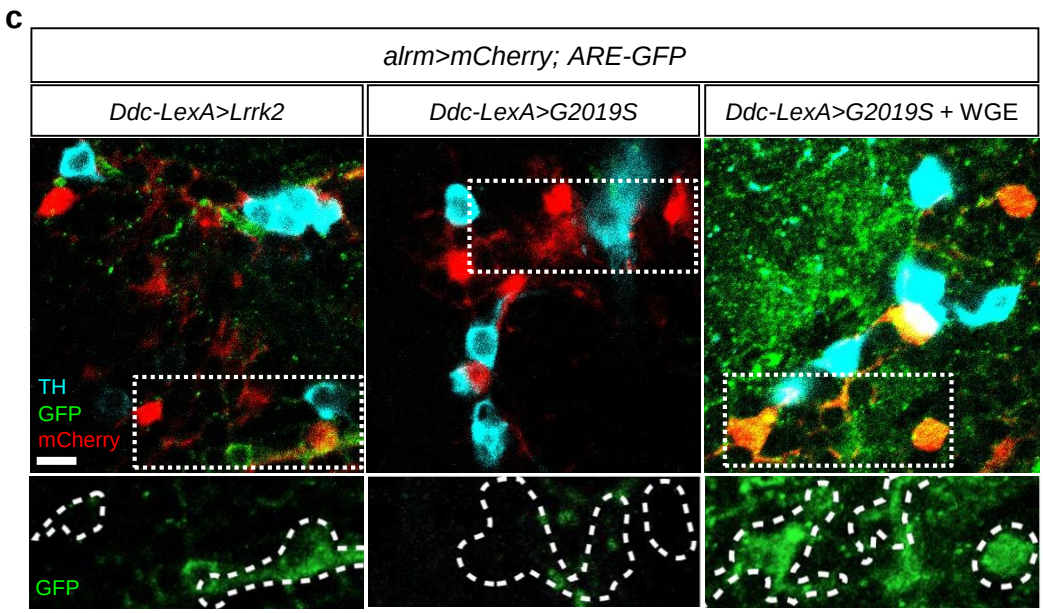
c
alrm>mCherry; ARE-GFP
Ddc-LexA>Lrrk2
Ddc-LexA>G2019S
Ddc-LexA>G2019S + WGE
TH
GFP
mCherry
GFP

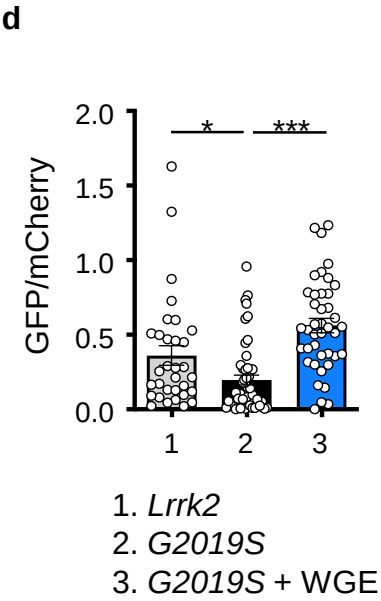
d
GFP/mCherry
2.0
1.5
1.0
0.5
0.0
*
***
1 2 3
1. Lrrk2
2. G2019S
3. G2019S + WGE

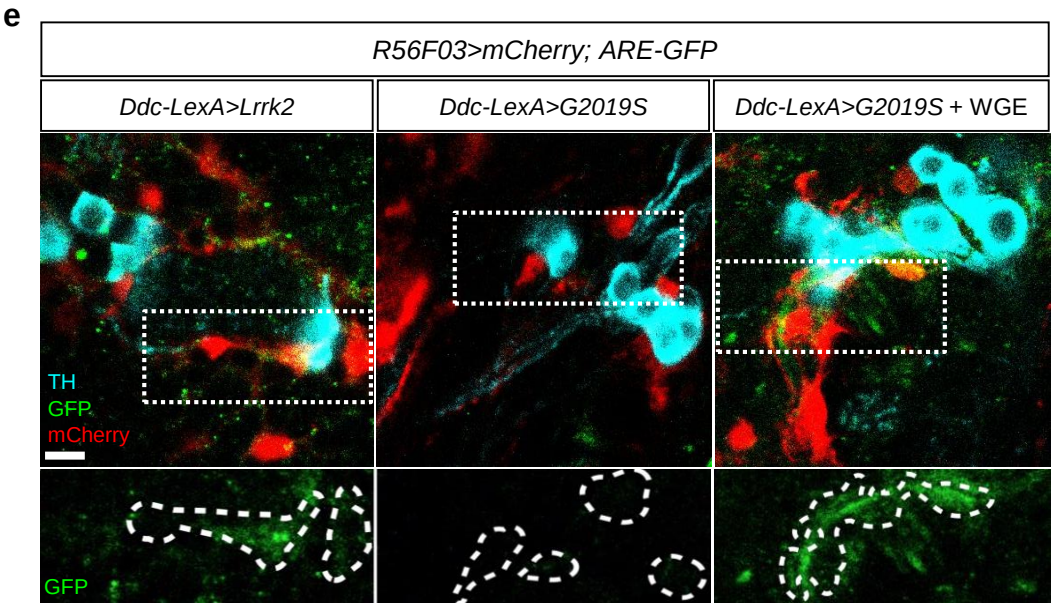
e
R56F03>mCherry; ARE-GFP
Ddc-LexA>Lrrk2
Ddc-LexA>G2019S
Ddc-LexA>G2019S + WGE
TH
GFP
mCherry
GFP

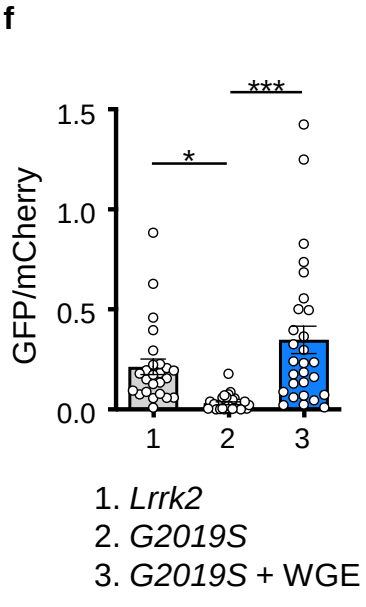
f
GFP/mCherry
1.5
1.0
0.5
0.0
*
***
1 2 3
1. Lrrk2
2. G2019S
3. G2019S + WGE

Fig. 7

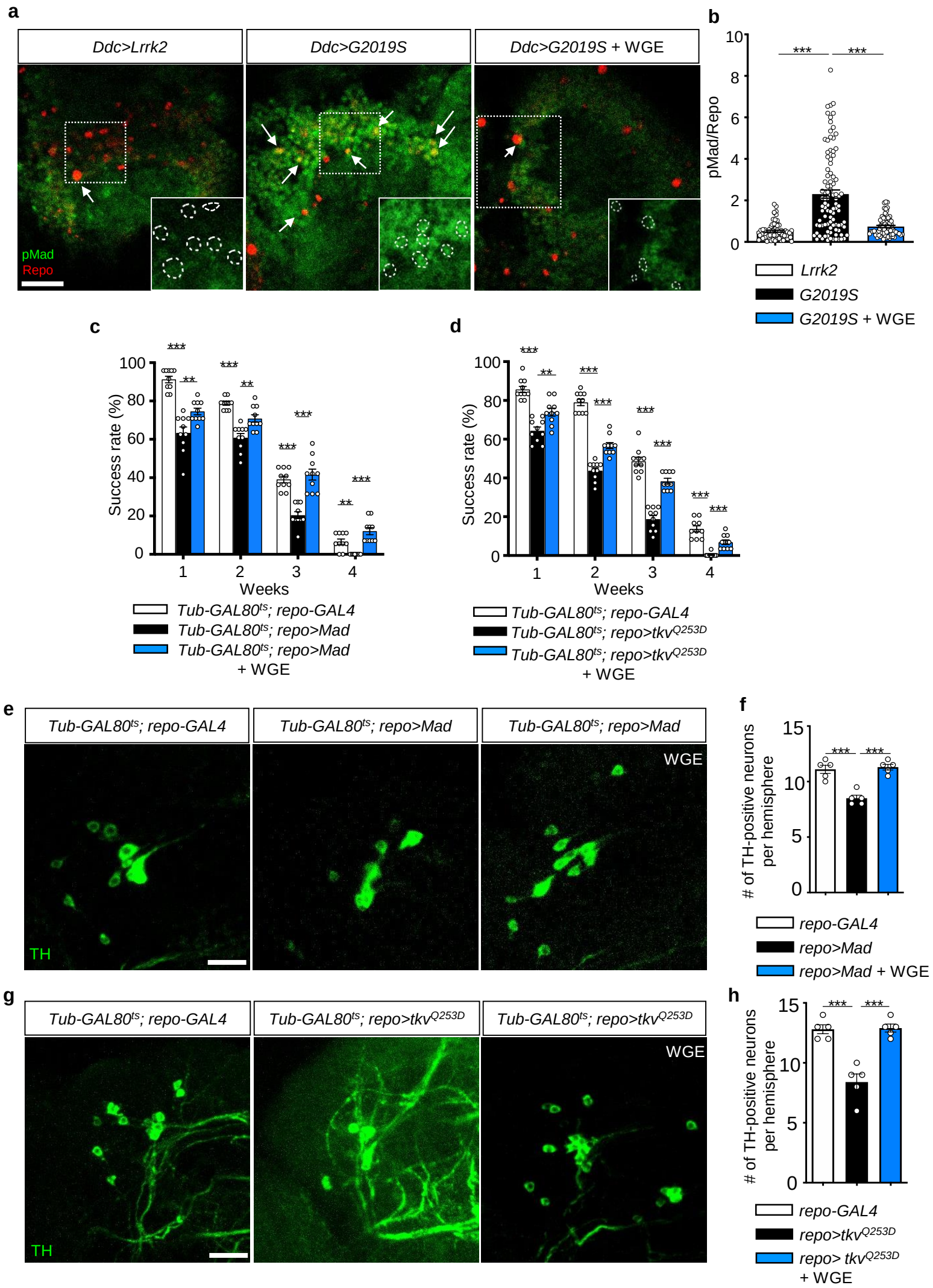
a
Ddc>Lrrk2
Ddc>G2019S
Ddc>G2019S + WGE
pMad
Repo
b
pMad/Repo
Lrrk2
G2019S
G2019S + WGE
c
Success rate (%)
Weeks
Tub-GAL80ts; repo-GAL4
Tub-GAL80ts; repo>Mad
Tub-GAL80ts; repo>Mad + WGE
d
Tub-GAL80ts; repo-GAL4
Tub-GAL80ts; repo>tkvQ253D
Tub-GAL80ts; repo>tkvQ253D + WGE
e
Tub-GAL80ts; repo-GAL4
Tub-GAL80ts; repo>Mad
Tub-GAL80ts; repo>Mad
WGE
TH
f
# of TH-positive neurons per hemisphere
repo-GAL4
repo>Mad
repo>Mad + WGE
g
Tub-GAL80ts; repo-GAL4
Tub-GAL80ts; repo>tkvQ253D
Tub-GAL80ts; repo>tkvQ253D
WGE
TH
h
# of TH-positive neurons per hemisphere
repo-GAL4
repo>tkvQ253D
repo> tkvQ253D + WGE

Fig. 8

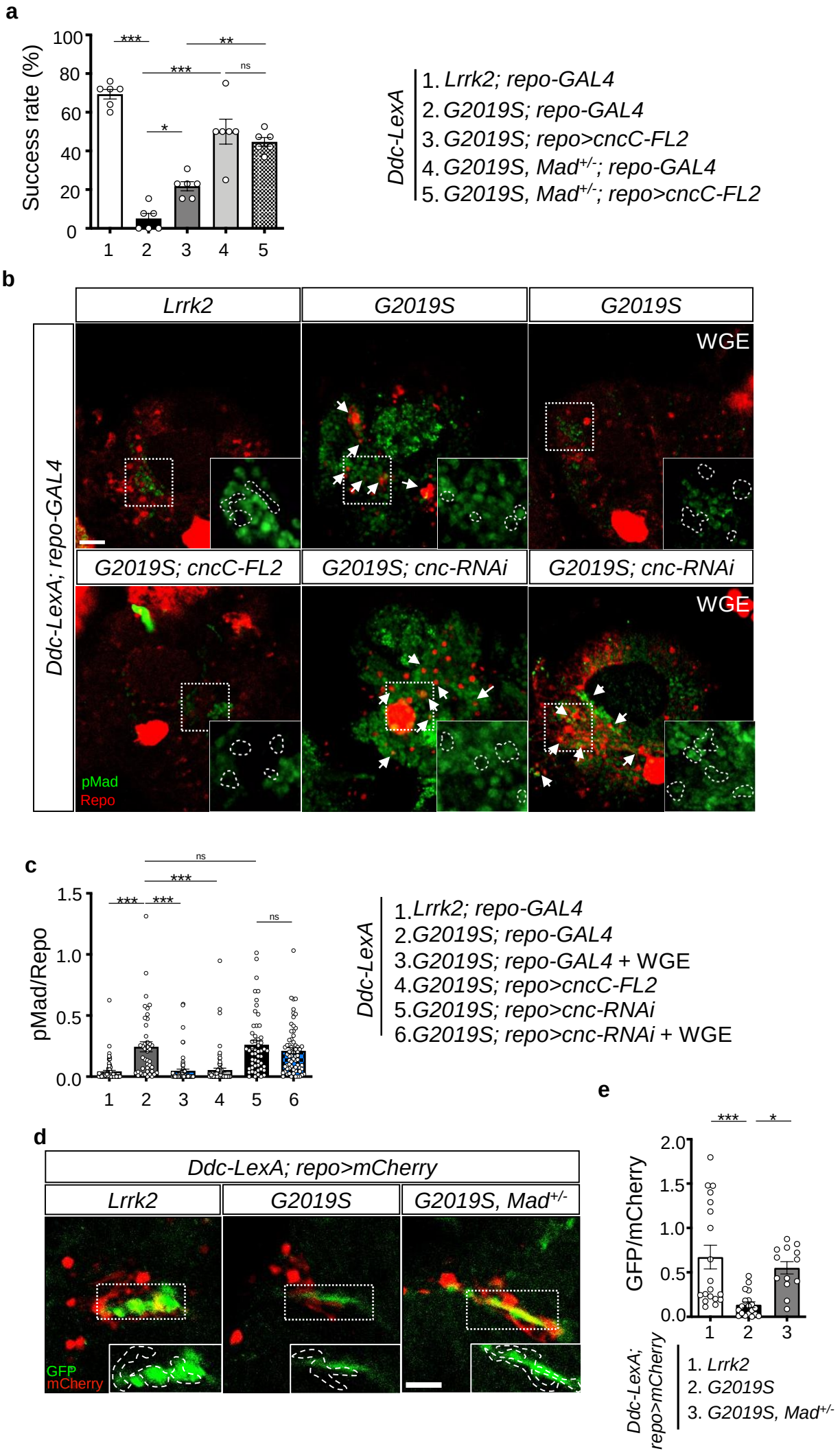
a
Success rate (%)
100
80
60
40
20
0
***
**
***
ns
*
1
2
3
4
5
Ddc-LexA
1. Lrrk2; repo-GAL4
2. G2019S; repo-GAL4
3. G2019S; repo>cncC-FL2
4. G2019S, Mad+/-; repo-GAL4
5. G2019S, Mad+/-; repo>cncC-FL2
b
Lrrk2
G2019S
G2019S
WGE
Ddc-LexA; repo-GAL4
G2019S; cncC-FL2
G2019S; cnc-RNAi
G2019S; cnc-RNAi
WGE
pMad
Repo
c
pMad/Repo
1.5
1.0
0.5
0.0
ns
***
***
***
ns
1
2
3
4
5
6
Ddc-LexA
1. Lrrk2; repo-GAL4
2. G2019S; repo-GAL4
3. G2019S; repo-GAL4 + WGE
4. G2019S; repo>cncC-FL2
5. G2019S; repo>cnc-RNAi
6. G2019S; repo>cnc-RNAi + WGE
d
Ddc-LexA; repo>mCherry
Lrrk2
G2019S
G2019S, Mad+/-
GFP
mCherry
e
GFP/mCherry
2.0
1.5
1.0
0.5
0.0
***
*
1
2
3
Ddc-LexA; repo>mCherry
1. Lrrk2
2. G2019S
3. G2019S, Mad+/-

Fig. 9

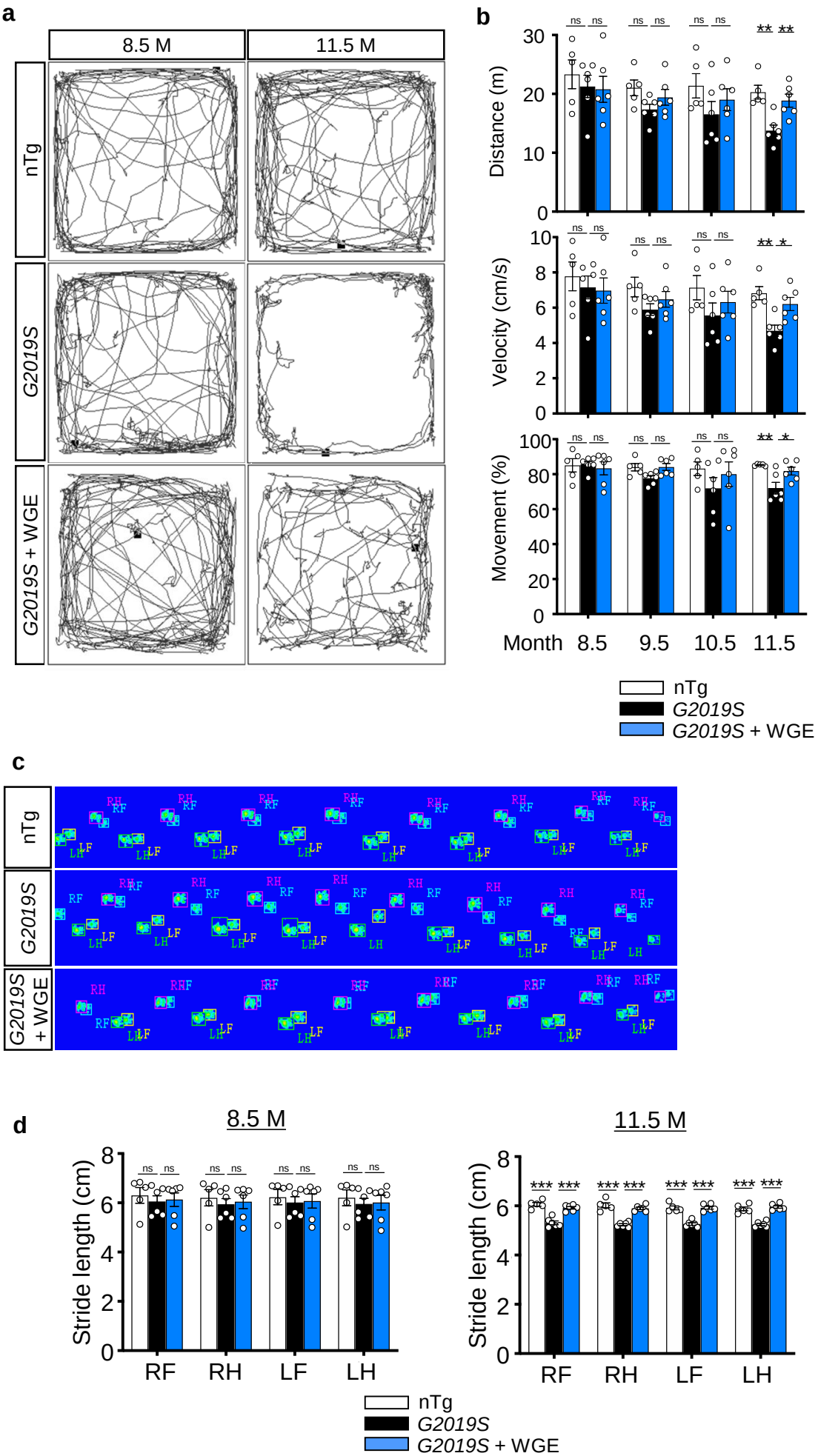
a
8.5 M
11.5 M
nTg
G2019S
G2019S + WGE
b
Distance (m)
Velocity (cm/s)
Movement (%)
Month 8.5 9.5 10.5 11.5
ns
**
*
nTg
G2019S
G2019S + WGE
c
nTg
G2019S
G2019S + WGE
RH
RF
LH
LF
d
8.5 M
11.5 M
Stride length (cm)
RF RH LF LH
***
nTg
G2019S
G2019S + WGE

Fig. 10

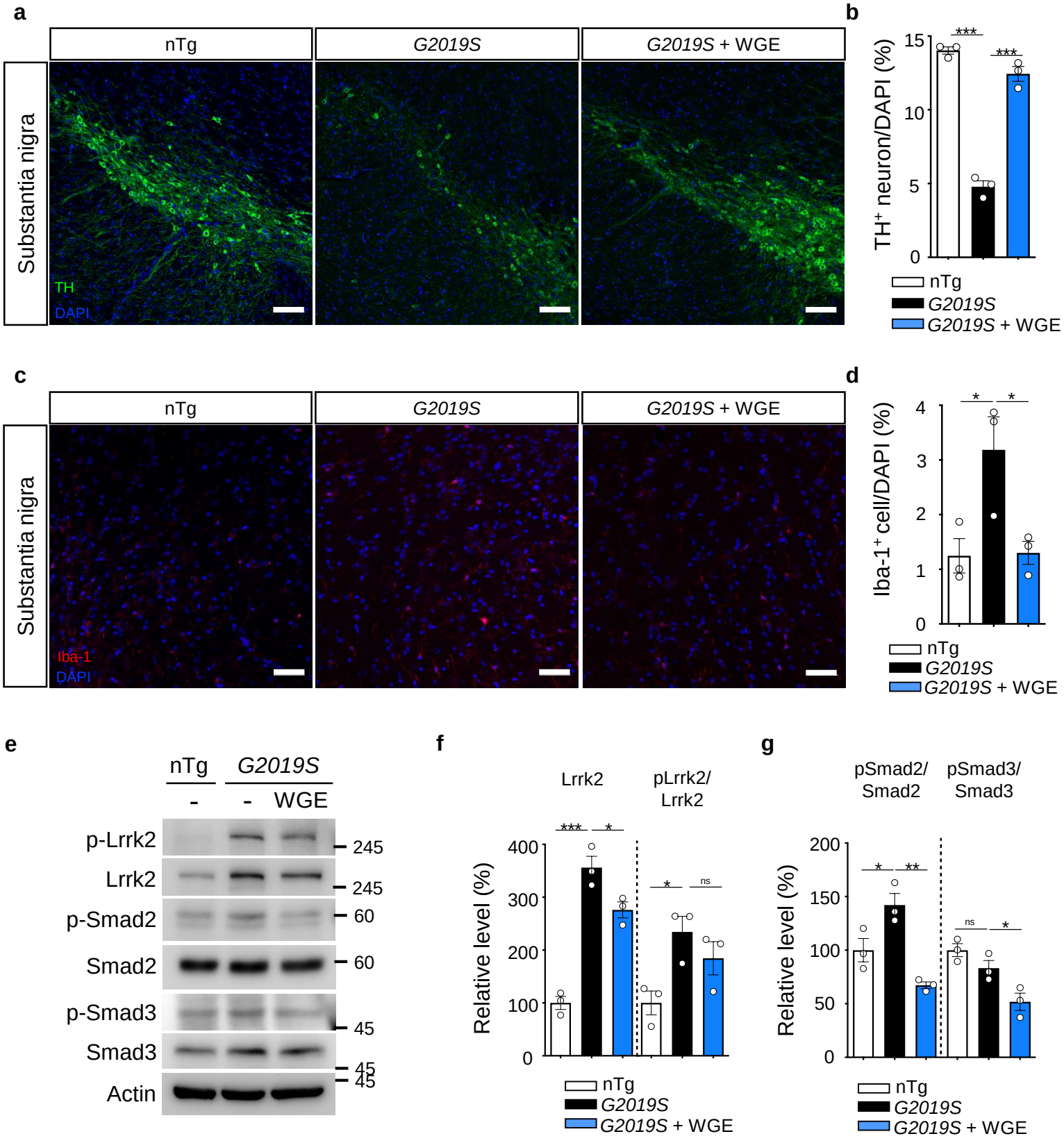
a
nTg
G2019S
G2019S + WGE
Substantia nigra
TH
DAPI
b
TH+ neuron/DAPI (%)
15
10
5
0
***
***
nTg
G2019S
G2019S + WGE
c
nTg
G2019S
G2019S + WGE
Substantia nigra
Iba-1
DAPI
d
Iba-1+ cell/DAPI (%)
4
3
2
1
0
*
*
nTg
G2019S
G2019S + WGE
e
nTg
G2019S
-
-
WGE
p-Lrrk2
Lrrk2
p-Smad2
Smad2
p-Smad3
Smad3
Actin
245
245
60
60
45
45
45
f
Lrrk2
pLrrk2/
Lrrk2
Relative level (%)
400
300
200
100
0
***
*
*
ns
nTg
G2019S
G2019S + WGE
g
pSmad2/
Smad2
pSmad3/
Smad3
Relative level (%)
200
150
100
50
0
*
**
ns
*
nTg
G2019S
G2019S + WGE